Journal of Scientific Computing
https://doi.org/10.1007/s10915-018-0837-0

Lowest-Order Weak Galerkin Finite Element Methods for Linear Elasticity on Rectangular and Brick Meshes

Graham Harper[1] · Jiangguo Liu[1] · Simon Tavener[1] · Bin Zheng[2]

Received: 1 December 2017 / Revised: 8 June 2018 / Accepted: 19 September 2018

Abstract
This paper investigates lowest-order weak Galerkin finite element methods for solving linear elasticity problems on rectangular and brick meshes. Specifically, constant vectors are used in element interiors and on element interfaces respectively for approximating displacement. For these constant basis functions, their discrete weak gradients are calculated in the local Raviart–Thomas spaces $RT^d_{[0]}$ ($d = 2$ or 3), whereas their discrete weak divergences are calculated as elementwise constants. Discrete weak strains are calculated accordingly. Then these quantities are used to develop finite element schemes in both strain-div and grad-div formulations, on both rectangular and brick meshes. A theoretical analysis supported by numerical experiments in both 2-dim and 3-dim reveal that the methods are locking-free and have optimal 1st order convergence in displacement, stress, and dilation (divergence of displacement), when the exact solution has full regularity. The methods can also capture low-regularity solutions very well. Strategies for efficient implementation including Schur complement are presented. Extension to quadrilateral and hexahedral meshes, in both theoretical analysis and numerical experiments, is also examined.

Keywords Brick meshes · Elasticity · Lowest-order finite elements · Rectangular meshes · Weak Galerkin (WG)

Mathematics Subject Classification 65N30 · 74B05

1 Introduction

This paper concerns finite element methods (FEMs) for linear elasticity problems formulated as

$$\begin{cases} -\nabla\cdot\sigma = \mathbf{f}(\mathbf{x}), \quad \mathbf{x}\in\Omega, \\ \mathbf{u}|_{\Gamma^D} = \mathbf{u}_D, \quad (-\sigma\mathbf{n})|_{\Gamma^N} = \mathbf{t}_N, \end{cases} \tag{1}$$

G. Harper was partially supported by US National Science Foundation (NSF) MSGI for 2017 summer internship at Pacific Northwest National Lab and NSF under Grants DMS-1419077 and DMS-1819252. J. Liu was partially supported by NSF under Grants DMS-1419077 and and DMS-1819252. S. Tavener was partially supported by NSF under Grant DMS-1720473.

✉ Jiangguo Liu
liu@math.colostate.edu

Extended author information available on the last page of the article

where Ω is a 2-dim or 3-dim bounded domain occupied by a homogeneous and isotropic elastic body, $\mathbf{f}$ is a body force, $\mathbf{u}_D$, $\mathbf{t}_N$ are respectively Dirichlet and Neumann data, $\mathbf{n}$ is the outward unit normal vector on the domain boundary $\partial\Omega = \Gamma^D \cup \Gamma^N$. As usual, $\mathbf{u}$ is the solid displacement,

$$\varepsilon(\mathbf{u}) = \frac{1}{2}\left(\nabla\mathbf{u} + (\nabla\mathbf{u})^T\right)$$

is the strain tensor, and

$$\sigma = 2\mu\ \varepsilon(\mathbf{u}) + \lambda(\nabla\cdot\mathbf{u})\mathbb{I},$$

is the Cauchy stress tensor, where $\mathbb{I}$ is the identity matrix of order two or three.

Note that the Lamé constants λ, μ are given by

$$\lambda = \frac{E\nu}{(1+\nu)(1-2\nu)}, \qquad \mu = \frac{E}{2(1+\nu)}, \tag{2}$$

where E is the elasticity modulus and ν is Poisson's ratio.

Let $L^2(\Omega)$, $H^1(\Omega)$ be the Sobolev spaces of scalar-valued functions and $\mathbf{L}^2(\Omega)$, $\mathbf{H}^1(\Omega)$, $\mathbf{H}^2(\Omega)$ be the Sobolev spaces of vector-valued functions. Let $\mathbf{H}^1_{D,0}(\Omega)$ be the subspace of functions in $\mathbf{H}^1(\Omega)$ whose values vanish on Γ^D. When $\Gamma^D = \partial\Omega$, we write $\mathbf{H}^1_{D,0}(\Omega)$ as $\mathbf{H}^1_0(\Omega)$.

The variational form in the strain-div formulation for (1) is to seek $\mathbf{u} \in \mathbf{H}^1(\Omega)$ such that $\mathbf{u}|_{\Gamma^D} = \mathbf{u}_D$ and

$$2\mu(\varepsilon(\mathbf{u}), \varepsilon(\mathbf{v})) + \lambda\big(\nabla\cdot\mathbf{u}, \nabla\cdot\mathbf{v}\big) = (\mathbf{f}, \mathbf{v}) - \langle\mathbf{t}_N, \mathbf{v}\rangle_{\Gamma^N}, \quad \forall\mathbf{v} \in \mathbf{H}^1_{D,0}(\Omega). \tag{3}$$

When a pure Dirichlet boundary condition is considered, we have $\Gamma^D = \partial\Omega$ and (1) can be reformulated as

$$\begin{cases} -\mu\Delta\mathbf{u} - (\mu+\lambda)\nabla(\nabla\cdot\mathbf{u}) = \mathbf{f}, \\ \mathbf{u}|_{\partial\Omega} = \mathbf{u}_D. \end{cases} \tag{4}$$

Accordingly, the variational form in the grad-div formulation is to seek $\mathbf{u} \in \mathbf{H}^1(\Omega)$ such that $\mathbf{u}|_{\Gamma^D} = \mathbf{u}_D$ and

$$\mu(\nabla\mathbf{u}, \nabla\mathbf{v}) + (\mu+\lambda)(\nabla\cdot\mathbf{u}, \nabla\cdot\mathbf{v}) = (\mathbf{f}, \mathbf{v}), \quad \forall\mathbf{v} \in \mathbf{H}^1_0(\Omega). \tag{5}$$

The regularity of the solution to problem (4) with homogeneous Dirichlet boundary conditions follows from [4,5]. When Ω is a convex polygon, there holds

$$\|\mathbf{u}\|_{\mathbf{H}^2(\Omega)} + \lambda\|\nabla\cdot\mathbf{u}\|_{H^1(\Omega)} \le C\|\mathbf{f}\|_{\mathbf{L}^2(\Omega)}, \tag{6}$$

where $C > 0$ is a constant independent of λ. Similar results for 3-dim can be found in [9].

A challenge in numerically solving linear elasticity is to overcome *Poisson-locking*. This locking is often manifested as loss of convergence rates in displacement and/or other quantities when $\lambda \to \infty$ or $\nu \to \frac{1}{2}$, that is, the material is nearly incompressible.

The development of efficient and robust finite element methods for linear elasticity on rectangular and brick meshes is an important problem in its own right. Some early efforts on locking-free FEMs for linear elasticity on two- and/or three-dimensional rectangular meshes can be found in [21,22]. These are nonconforming mixed finite element methods (MFEMs) based on the Hellinger–Reissner formulation. A recent work in this direction [8] develops finite elements with the least number of degrees of freedom.

A closely related topic is the investigation of finite elements on quadrilateral and hexahedral meshes. Some early efforts to construct locking-free nonconforming finite elements for linear elasticity on general quadrilaterals can be found in [16,24]. Mixed finite elements on quadrilaterals can be found in [2] and reference therein. In [10], a mixed finite element method (MFEM) is developed for nearly incompressible elasticity (and also Stokes flow) using primal and dual meshes with quadrilateral and hexahedral grids. For the MFEMs in the displacement-pressure formulation, a biorthogonal system is developed in [11] so that the pressure degrees of freedom can be statically condensed and the MFEMs become much more efficient. It is unclear whether such a technique applies to the FEMs based on the stress-displacement formulation.

Recently, the weak Galerkin (WG) methodology has emerged with some interesting features. WGFEMs have been developed for several types of partial differential equations. A family of WGFEMs for the linear elasticity equation on polygonal meshes was developed in [18]. These methods use degree $k \geq 1$ vector polynomials for element interiors but degree $k-1$ vector polynomials for element interfaces, and a penalization term is necessary. Order $k+1$ accuracy is attained for displacement, but only order k accuracy can be expected for stress and dilation.

In this paper, we develop the lowest-order weak Galerkin finite element methods for linear elasticity on rectangular and brick meshes. Namely, constant vectors are used in element interiors and on inter-element boundaries for approximating displacement. No penalization is needed. The methods have optimal first order accuracy in displacement, stress, and dilation, when the exact solution has full regularity. The new methods can also capture low regularity solutions very well and can be extended to quadrilateral and hexahedral meshes.

The rest of this paper is organized as follows. Section 2 introduces the basic concepts of weak Galerkin and presents the new finite element methods in both strain-div and grad-div formulations. Section 3 presents a theoretical analysis on rectangular meshes and examines also the extension to quadrilateral meshes. Section 4 discusses implementation and the Schur complement. Section 5 briefly reviews an existing WG method in [18]. Section 6 presents test cases in two and three dimensions in order to demonstrate the important features of our new methods, namely locking-free and optimal order convergence, the ability to accurately capture low regularity solutions and the cost reduction achieved through the use of the Schur complement.

2 Lowest-Order WGFEMs for Elasticity on Rectangular and Brick Meshes

This paper develops the lowest-order weak Galerkin finite element methods

- WG(Q_0^2, Q_0^2; $RT_{[0]}^2$, Q_0) on rectangular meshes,
- WG(Q_0^3, Q_0^3; $RT_{[0]}^3$, Q_0) on brick meshes

for linear elasticity problems. In either case, the displacement is approximated by constant vectors in element interiors and on edges/faces.

The main ideas in the weak Galerkin finite element methodology are as follows.

(i) Choose basis functions separately for element interiors and for inter-element boundaries (or the mesh skeleton). These can be polynomials of different degrees. For example, on a rectangle E, one can use Q_0^2 (constant vectors) separately for its interior E° and boundary E^∂.

(ii) Specify the discrete weak gradients or divergences of the above basis functions in (known) spaces that have desired approximation capacity. This is established through

integration by parts. For example, for a rectangle E, we can use the matrix-version Raviart–Thomas space $RT^2_{[0]}(E)$ for discrete weak gradients and simply $Q_0(E)$ for discrete weak divergences.

(iii) Use the aforementioned basis functions to approximate the physical variable in a given problem, e.g., displacement in elasticity. Use the discrete weak gradients or divergences to approximate the classical gradient or divergence in the variational form of the given problem, for example, the strain-div formulation (3).

For detailed discussion of general concepts of weak functions, weak different operators (gradient, divergence, curl), discrete weak functions, discrete weak gradients (divergences, curls), the reader is referred to [18,19].

2.1 WG(Q_0^2, Q_0^2; $RT^2_{[0]}$, Q_0) Scheme for Elasticity on Rectangular Meshes

Let E be a rectangle and (x_c, y_c) be its center. Let $X = x - x_c$, $Y = y - y_c$ be the normalized coordinates.

Recall that the Raviart–Thomas space $RT_0(E)$ consists of vector-valued functions whose first components are linear functions of the first coordinate and whose second components are linear in the second coordinate [6]. Accordingly, $RT_0^2(E)$ consists of functions that are order two square matrices with row vectors in $RT_{[0]}(E)$.

Note that the local space $RT^2_{[0]}(E)$ can be generated by the following eight basis functions [15]:

$$\begin{aligned} W_1 &= \begin{bmatrix} 1 & 0 \\ 0 & 0 \end{bmatrix}, \ W_2 = \begin{bmatrix} 0 & 1 \\ 0 & 0 \end{bmatrix}, \ W_3 = \begin{bmatrix} X & 0 \\ 0 & 0 \end{bmatrix}, \ W_4 = \begin{bmatrix} 0 & Y \\ 0 & 0 \end{bmatrix}, \\ W_5 &= \begin{bmatrix} 0 & 0 \\ 1 & 0 \end{bmatrix}, \ W_6 = \begin{bmatrix} 0 & 0 \\ 0 & 1 \end{bmatrix}, \ W_7 = \begin{bmatrix} 0 & 0 \\ X & 0 \end{bmatrix}, \ W_8 = \begin{bmatrix} 0 & 0 \\ 0 & Y \end{bmatrix}. \end{aligned} \tag{7}$$

Their Gram matrix is an 8×8 symmetric positive-definite (SPD) matrix.

Next we consider WG(Q_0^2, Q_0^2)-type vector-valued discrete weak functions on a rectangle E. Such a function $\mathbf{v} = \{\mathbf{v}^\circ, \mathbf{v}^\partial\}$ has two parts: $\mathbf{v}^\circ$ denotes its value as a constant vector in the element interior E°; $\mathbf{v}^\partial$ denotes its value on the element boundary E^∂, the value is a constant vector on each edge of the boundary. The 10 basis functions are as follows.

- For the interior E°, there are 2 basis functions $\mathbf{v}_1, \mathbf{v}_2$ such that their values in the element interior are $\mathbf{v}_1^\circ = \begin{bmatrix} 1 \\ 0 \end{bmatrix}, \mathbf{v}_2^\circ = \begin{bmatrix} 0 \\ 1 \end{bmatrix}$. However, their values $\mathbf{v}_1^\partial, \mathbf{v}_2^\partial$ on the boundary E^∂ are the zero vector.
- For the i-th ($1 \le i \le 4$) edge, there are also 2 basis functions $\mathbf{v}_{2i+1}, \mathbf{v}_{2i+2}$ such that $\mathbf{v}_{2i+1}^\partial = \begin{bmatrix} 1 \\ 0 \end{bmatrix}, \mathbf{v}_{2i+2}^\partial = \begin{bmatrix} 0 \\ 1 \end{bmatrix}$ on the edge itself, but their values are the zero vector on all other edges and also in the element interior.

Let $\mathbf{v} = \{\mathbf{v}^\circ, \mathbf{v}^\partial\}$ be a WG(Q_0^2, Q_0^2)-type discrete weak function. We specify its *discrete weak gradient* $\nabla_{w,d}\phi$ in $RT^2_{[0]}(E)$ via integration by parts

$$\int_E \big(\nabla_{w,d}\mathbf{v}\big) : W = \int_{E^\partial} \mathbf{v}^\partial \cdot (W\mathbf{n}) - \int_{E^\circ} \mathbf{v}^\circ \cdot \big(\nabla \cdot W\big), \quad \forall W \in RT^2_{[0]}(E), \tag{8}$$

where : is the standard colon product for matrices and $\mathbf{n}$ is the outward unit vector on the element boundary E^∂. If we set $\nabla_{w,d}\mathbf{v} = \sum_{j=1}^8 c_j W_j$, then these eight coefficients $c_1, \ldots, c_8$

are obtained by solving a SPD linear system that has the aforementioned Gram matrix as the coefficient matrix.

The *discrete weak strain* of such a discrete weak function $\mathbf{v}$ is defined as

$$\varepsilon_{w,d}(\mathbf{v}) = \frac{1}{2}\left(\nabla_{w,d}\mathbf{v} + \left(\nabla_{w,d}\mathbf{v}\right)^T\right). \tag{9}$$

The *discrete weak divergence* $\nabla_{w,d}\cdot\mathbf{v}$ of such a discrete weak function $\mathbf{v}$ is also defined via integration by parts

$$\int_E \left(\nabla_{w,d}\cdot\mathbf{v}\right)w = \int_{E^\partial} \mathbf{v}^\partial\cdot(w\mathbf{n}) - \int_{E^\circ}\mathbf{v}^\circ\cdot\left(\nabla w\right), \quad \forall w\in Q^0(E). \tag{10}$$

Note that the second term on the right-hand side of the above equation disappears since the classical gradient of a constant function is a zero vector, and hence the discrete weak divergence can be computed directly.

Let $\mathcal{E}_h$ be a quasi-uniform rectangular mesh. Let Γ_h^D be the set of all edges along the Dirichlet boundary Γ^D. Similarly, let Γ_h^N be the set of all edges on Γ^N. Let V_h be the space of all WG(Q_0^2, Q_0^2)-type discrete weak functions on the whole mesh $\mathcal{E}_h$, namely, their values in element interiors are constant vectors, and their values on edges are also constant vectors. Note that this global finite element space is obtained by gluing the local weak functions through the inter-element boundaries (mesh skeleton). Furthermore, let V_h^0 be the subspace of discrete weak functions in V_h whose values vanish on the Dirichlet edges (Γ_h^D). Let $\mathbf{Q}_h^\partial$ be a local L_2-projection to the space of constant vectors on edges.

WG finite element scheme in strain-div formulation. The weak Galerkin $(Q_0^2, Q_0^2; RT_{[0]}^2, Q_0)$ scheme in the strain-div formulation for the linear elasticity problem (1) is formulated as: Seek $\mathbf{u}_h\in V_h$ such that $\mathbf{u}_h|_{\Gamma_h^D} = \mathbf{Q}_h^\partial(\mathbf{u}_D)$ and

$$\mathcal{A}_h^{SD}(\mathbf{u}_h,\mathbf{v}) = \mathcal{F}_h^{SD}(\mathbf{v}), \qquad \forall\mathbf{v}\in V_h^0, \tag{11}$$

where

$$\begin{aligned}\mathcal{A}_h^{SD}(\mathbf{u}_h,\mathbf{v}) = 2\mu&\sum_{E\in\mathcal{E}_h}(\varepsilon_{w,d}(\mathbf{u}_h),\varepsilon_{w,d}(\mathbf{v}))_E\\ &+\lambda\sum_{E\in\mathcal{E}_h}\left(\nabla_{w,d}\cdot\mathbf{u}_h,\nabla_{w,d}\cdot\mathbf{v}\right)_E,\end{aligned} \tag{12}$$

and

$$\mathcal{F}_h^{SD}(\mathbf{v}) = \sum_{E\in\mathcal{E}_h}(\mathbf{f},\mathbf{v}^\circ)_E - \sum_{\gamma\in\Gamma_h^N}\langle\mathbf{t}_N,\mathbf{v}^\partial\rangle_\gamma. \tag{13}$$

WG finite element scheme in grad-div formulation. The weak Galerkin $(Q_0^2, Q_0^2; RT_{[0]}^2, Q_0)$ scheme in the grad-div formulation for the linear elasticity problem (4) is formulated as: Seek $\mathbf{u}_h\in V_h$ such that $\mathbf{u}_h|_{\Gamma_h^D} = \mathbf{Q}_h^\partial(\mathbf{u}_D)$ and

$$\mathcal{A}_h^{GD}(\mathbf{u}_h,\mathbf{v}) = \mathcal{F}_h^{GD}(\mathbf{v}), \qquad \forall\mathbf{v}\in V_h^0, \tag{14}$$

where

$$\begin{aligned}\mathcal{A}_h^{GD}(\mathbf{u}_h,\mathbf{v}) = \mu&\sum_{E\in\mathcal{E}_h}\left(\nabla_{w,d}\mathbf{u}_h,\nabla_{w,d}\mathbf{v}\right)_E\\ &+\left(\mu+\lambda\right)\sum_{E\in\mathcal{E}_h}\left(\nabla_{w,d}\cdot\mathbf{u}_h,\nabla_{w,d}\cdot\mathbf{v}\right)_E,\end{aligned} \tag{15}$$

and

$$\mathcal{F}_h^{GD}(\mathbf{v}) = \sum_{E\in\mathcal{E}_h} (\mathbf{f}, \mathbf{v}^\circ)_E. \tag{16}$$

Remarks (i) No penalization is needed for these two WG finite element schemes.
(ii) These two schemes can be extended to a quadrilateral mesh with $RT_{[0]}$ being the unmapped local Raviart–Thomas space. See the end of Sect. 3 for a discussion.

2.2 WG(Q_0^3, Q_0^3; $RT_{[0]}^3$, Q_0) Scheme for Elasticity on Brick Meshes

In the same spirit, WG(Q_0^3, Q_0^3; $RT_{[0]}^3$, Q_0) finite element schemes can be developed in both strain-div and grad-div formulations for linear elasticity on a brick (3-dim rectangular) mesh. The schemes take the same forms as those shown in (11) and (14).

Let E be a brick (3-dim rectangle) with center (x_c, y_c, z_c). Let $X = x - x_c, Y = y - y_c, Z = z - z_c$ be the normalized coordinates. Now $\dim(RT_{[0]}^3(E)) = 18$ for the local lowest-order Raviart–Thomas space on the brick. We still use the lowest-order WG basis functions (Q_0^3, Q_0^3). Specifically, we have three constant vector basis functions for the interior E°, and also three functions for each of the six faces that consists of the boundary E^∂. This results in 21 degrees of freedom elementwise for displacement. For these 21 WG basis functions, their discrete weak gradients are obtained in $RT_{[0]}^3(E)$ by solving size-18 SPD linear systems, whereas their discrete weak divergences are calculated directly as constants. Their discrete weak strains can then be calculated. These quantities are then applied in 3-dim finite element schemes that are similar to (11) or (14) for solving displacement. Similarly, these schemes can be readily extended to a hexahedral mesh.

3 Analysis

For ease of presentation, our error analysis focuses on the finite element scheme (14) for problem (4) with homogeneous Dirichlet boundary conditions. We consider the grad-div formulation on a rectangular mesh. For convenience, we use $A \lesssim B$ to simplify an inequality $A \le CB$ when $C > 0$ is a constant independent of h and λ.

Let $\mathcal{E}_h$ be a quasi-uniform rectangular mesh. Our weak Galerkin shape functions are taken from V_h or V_h^0. We also require the following auxiliary space,

$$W_h = \{q : q|_E \in Q^0(E), \forall E \in \mathcal{E}_h\}. \tag{17}$$

Definition 1 (*Semi-norm on V_h*). For $\mathbf{v} \in V_h$, we define

$$|||\mathbf{v}|||^2 = \sum_{E\in\mathcal{E}_h} h_E^{-1} \|\mathbf{v}^\partial - \mathbf{v}^\circ\|_{E^\partial}^2. \tag{18}$$

For ease of presentation, there is a mild abuse of the notation $\mathbf{v}^\circ$ in the above formula. In fact we extend $\mathbf{v}^\circ$ to the element boundary using the same constant vector. Similar interpretations apply to Lemmas 2, 4, 5, 6, 7 and Theorems 1, 2, and their proofs.

Remarks (i) This is essentially a gradient in the discrete sense for these lowest-order discrete weak functions;
(ii) If higher order WG basis functions $(Q_k^2, Q_k^2)(k \ge 1)$ are used, we need to add another term to (18), e.g., $\nabla\mathbf{v}^\circ$, for the classical gradient of its interior part, see also [18].

Lemma 0 *The above semi-norm becomes a norm on* V_h^0. □

Definition 2 (*Local projection operators*). Let E be a rectangle. We define

(i) Q_h as the L^2-projection from $L^2(E)$ to the space of constant scalars on E;
(ii) $\mathbf{Q}_h = \{\mathbf{Q}_h^\circ, \mathbf{Q}_h^\partial\}$, where $\mathbf{Q}_h^\circ$ is the local L^2-projection from $\mathbf{L}^2(E^\circ)$ to the space of constant vectors on E°, whereas $\mathbf{Q}_h^\partial$ is the local L^2-projection from $\mathbf{L}^2(E^\partial)$ to the space of piecewise constant vectors on E^∂;
(iii) $\mathbb{Q}_h$ as the local L^2-projection from $L^2(E)^{2\times 2}$ to the space $RT_{[0]}^2(E)$.

Lemma 1 (Commuting identities). *Let* $E \in \mathcal{E}_h$.

(i) *For* $\mathbf{u} \in \mathbf{H}^1(E)$, *there holds* $\nabla_{w,d}(\mathbf{Q}_h\mathbf{u}) = \mathbb{Q}_h(\nabla\mathbf{u})$;
(ii) *For* $\mathbf{u} \in H(div, E)$, *there holds* $\nabla_{w,d} \cdot (\mathbf{Q}_h\mathbf{u}) = Q_h(\nabla \cdot \mathbf{u})$.

Proof Apply the definitions of the discrete weak gradient and discrete weak divergence, the definitions of the above local projections, and Gauss Divergence Theorem. □

Lemma 2 (Conversion to trace). *Let* $E \in \mathcal{E}_h$ *and* $\mathbf{v} \in V_h$.

(i) *For any* $W \in RT_{[0]}^2(E)$, *there holds*

$$\big(W, \nabla_{w,d}\mathbf{v}\big)_E = \big\langle W\mathbf{n}, \mathbf{v}^\partial - \mathbf{v}^\circ\big\rangle_{E^\partial}. \tag{19}$$

(ii) *For any* $w \in W_h$, *there holds*

$$\big(w, \nabla_{w,d} \cdot \mathbf{v}\big)_E = \big\langle w\mathbf{n}, \mathbf{v}^\partial - \mathbf{v}^\circ\big\rangle_{E^\partial}. \tag{20}$$

Proof Apply the definitions of the discrete weak gradient and discrete weak divergence, and Gauss Divergence Theorem. □

Lemma 3 (Trace equivalence for $RT_{[0]}^2$). *For* $E \in \mathcal{E}_h$, *there holds*

$$\|W\mathbf{n}\|_{E^\partial}^2 \approx h_E^{-1}\|W\|_E^2, \qquad \forall W \in RT_{[0]}^2(E). \tag{21}$$

Proof It can be proved using the techniques in [6] that

$$\|\mathbf{w} \cdot \mathbf{n}\|_{E^\partial}^2 \approx h_E^{-1}\|\mathbf{w}\|_E^2, \qquad \forall \mathbf{w} \in RT_{[0]}(E),$$

where the equivalence holds with absolute constants that are independent of the mesh size. The result in (21) is a matrix version of this equivalence. □

Lemma 4 (Coercivity). *There holds*

$$|\|\mathbf{v}\|| \lesssim \|\nabla_{w,d}\mathbf{v}\|, \qquad \forall \mathbf{v} \in V_h^0. \tag{22}$$

Proof Let $\mathbf{v} \in V_h^0$. Consider any fixed rectangle E. Since there are 8 coefficients in W and $\mathbf{v}^\partial$ offers 8 constant vectors on all 4 edges together, there exists $W \in RT_{[0]}^2(E)$ such that $(W\mathbf{n})|_{E^\partial} = \mathbf{v}^\partial - \mathbf{v}^\circ$. Then applying Lemma 2(i) yields

$$\big\|\mathbf{v}^\partial - \mathbf{v}^\circ\big\|_{E^\partial}^2 = (W, \nabla_{w,d}\mathbf{v})_E.$$

By the Cauchy–Schwarz and Young's inequalities, we have, for any $\delta > 0$,

$$\big\|\mathbf{v}^\partial - \mathbf{v}^\circ\big\|_{E^\partial}^2 \le \frac{\delta}{2}\|W\|_E^2 + \frac{1}{2\delta}\big\|\nabla_{w,d}\mathbf{v}\big\|_E^2.$$

By the trace equivalence in (21), there exists an absolute constant C such that

$$\|W\|_E^2 \leq Ch_E \|W\mathbf{n}\|_{E^\partial}^2.$$

So we have

$$\left\|\mathbf{v}^\partial - \mathbf{v}^\circ\right\|_{E^\partial}^2 \leq \frac{\delta}{2} Ch_E \left\|\mathbf{v}^\partial - \mathbf{v}^\circ\right\|_{E^\partial}^2 + \frac{1}{2\delta}\left\|\nabla_{w,d}\mathbf{v}\right\|_E^2.$$

Rearranging terms yields

$$2\delta\Big(1 - \frac{\delta}{2}Ch_E\Big)\left\|\mathbf{v}^\partial - \mathbf{v}^\circ\right\|_{E^\partial}^2 \leq \left\|\nabla_{w,d}\mathbf{v}\right\|_E^2.$$

By choosing $\delta = 1/(Ch_E)$, we obtain

$$C^{-1}h_E^{-1}\left\|\mathbf{v}^\partial - \mathbf{v}^\circ\right\|_{E^\partial}^2 \leq \left\|\nabla_{w,d}\mathbf{v}\right\|_E^2.$$

Summing the above estimate over the entire mesh yields the desired result. □

Lemma 5 (Boundedness). *Assume* $\mathbf{v} \in V_h$ *and* $E \in \mathcal{E}_h$. *Then*

$$\left\|\nabla_{w,d}\mathbf{v}\right\|_E^2 \lesssim h_E^{-1}\left\|\mathbf{v}^\partial - \mathbf{v}^\circ\right\|_{E^\partial}^2. \tag{23}$$

and

$$\left\|\nabla_{w,d}\cdot\mathbf{v}\right\|_E^2 \lesssim h_E^{-1}\left\|\mathbf{v}^\partial - \mathbf{v}^\circ\right\|_{E^\partial}^2. \tag{24}$$

Proof For the first inequality, we proceed as follows: take $W = \nabla_{w,d}\mathbf{v}$ in Lemma 2(i), then apply the Cauchy–Schwarz inequality, Lemma 3 (trace equivalence) and an elementary (Young's) inequality to obtain

$$\begin{aligned}
\left\|\nabla_{w,d}\mathbf{v}\right\|_E^2 &= \langle(\nabla_{w,d}\mathbf{v})\mathbf{n}, \mathbf{v}^\partial - \mathbf{v}^\circ\rangle_{E^\partial} \\
&\leq \left\|(\nabla_{w,d}\mathbf{v})\mathbf{n}\right\|_{E^\partial}\left\|\mathbf{v}^\partial - \mathbf{v}^\circ\right\|_{E^\partial} \\
&\leq Ch_E^{-\frac{1}{2}}\left\|\nabla_{w,d}\mathbf{v}\right\|_E\left\|\mathbf{v}^\partial - \mathbf{v}^\circ\right\|_{E^\partial} \\
&\leq \frac{1}{2}\left\|\nabla_{w,d}\mathbf{v}\right\|_E^2 + \frac{1}{2}C^2h_E^{-1}\left\|\mathbf{v}^\partial - \mathbf{v}^\circ\right\|_{E^\partial}^2.
\end{aligned}$$

Rearranging terms yields

$$\left\|\nabla_{w,d}\mathbf{v}\right\|_E^2 \leq C^2h_E^{-1}\left\|\mathbf{v}^\partial - \mathbf{v}^\circ\right\|_{E^\partial}^2.$$

The second inequality can be proven in a similar way using the quasi-uniformity of the mesh, which says essentially that $|E|/|E^\partial| \approx h$. □

Lemma 6 (Error equation). *Let* $\mathbf{u}_h$ *be the numerical solution from* (14) *with a homogeneous Dirichlet boundary condition. Let* $\mathbf{u}$ *be the exact solution of* (4). *There holds*

$$\mathcal{A}_h^{GD}(\mathbf{u}_h - \mathbf{Q}_h\mathbf{u}, \mathbf{v}) = \mu\,\mathcal{G}_1(\mathbf{u}, \mathbf{v}) + (\mu + \lambda)\,\mathcal{G}_2(\mathbf{u}, \mathbf{v}), \tag{25}$$

where

$$\mathcal{G}_1(\mathbf{u}, \mathbf{v}) = \sum_{E\in\mathcal{E}_h}\left\langle(\nabla\mathbf{u} - \mathbb{Q}_h(\nabla\mathbf{u}))\mathbf{n}, \mathbf{v}^\partial - \mathbf{v}^\circ\right\rangle_{E^\partial}, \tag{26}$$

and

$$\mathcal{G}_2(\mathbf{u}, \mathbf{v}) = \sum_{E\in\mathcal{E}_h}\left\langle(\nabla\cdot\mathbf{u} - Q_h(\nabla\cdot\mathbf{u}))\mathbf{n}, \mathbf{v}^\partial - \mathbf{v}^\circ\right\rangle_{E^\partial}. \tag{27}$$

Proof Let $\mathbf{v} = \{\mathbf{v}^\circ, \mathbf{v}^\partial\} \in V_h$ and $E \in \mathcal{E}_h$. Using the differential equation in (4) and integration by parts, we have

$$\begin{aligned}\big(\mathbf{f}, \mathbf{v}^\circ\big)_E &= -\mu\big(\Delta\mathbf{u}, \mathbf{v}^\circ\big)_E - (\mu+\lambda)\big(\nabla(\nabla\cdot\mathbf{u}), \mathbf{v}^\circ\big)_E \\ &= -\mu\big\langle(\nabla\mathbf{u})\mathbf{n}, \mathbf{v}^\circ\big\rangle_{E^\partial} + \mu\big(\nabla\mathbf{u}, \nabla\mathbf{v}^\circ\big)_E \\ &\quad - (\mu+\lambda)\big\langle(\nabla\cdot\mathbf{u})\mathbf{n}, \mathbf{v}^\circ\big\rangle_{E^\partial} + (\mu+\lambda)\big(\nabla\cdot\mathbf{u}, \nabla\cdot\mathbf{v}^\circ\big)_E.\end{aligned}$$

Since $\mathbf{v}^\circ$ is an elementwise constant vector, $\nabla\mathbf{v}^\circ = \mathbf{0}$ and $\nabla\cdot\mathbf{v}^\circ = 0$. Therefore, the previous expression can be simplified as

$$\big(\mathbf{f}, \mathbf{v}^\circ\big)_E = -\mu\big\langle(\nabla\mathbf{u})\mathbf{n}, \mathbf{v}^\circ\big\rangle_{E^\partial} - (\mu+\lambda)\big\langle(\nabla\cdot\mathbf{u})\mathbf{n}, \mathbf{v}^\circ\big\rangle_{E^\partial}. \tag{28}$$

Under the assumptions of normal continuity of the exact solution and homogeneous boundary conditions, we have

$$\sum_{E\in\mathcal{E}_h}\big\langle(\nabla\mathbf{u})\mathbf{n}, \mathbf{v}^\partial\big\rangle_{E^\partial} = 0, \qquad \sum_{E\in\mathcal{E}_h}\big\langle(\nabla\cdot\mathbf{u})\mathbf{n}, \mathbf{v}^\partial\big\rangle_{E^\partial} = 0. \tag{29}$$

Combining these with (28) and the finite element scheme (14) gives

$$\begin{aligned}\mathcal{A}_h^{GD}(\mathbf{u}_h, \mathbf{v}) = \sum_{E\in\mathcal{E}_h}\big(\mathbf{f}, \mathbf{v}^\circ\big)_E &= \mu\sum_{E\in\mathcal{E}_h}\big\langle(\nabla\mathbf{u})\mathbf{n}, \mathbf{v}^\partial - \mathbf{v}^\circ\big\rangle_{E^\partial} \\ &\quad + (\mu+\lambda)\sum_{E\in\mathcal{E}_h}\big\langle(\nabla\cdot\mathbf{u})\mathbf{n}, \mathbf{v}^\partial - \mathbf{v}^\circ\big\rangle_{E^\partial}.\end{aligned} \tag{30}$$

On the other hand, by the commuting identities in Lemma 1 and the conversion formulas in Lemma 2, we have

$$\big(\nabla_{w,d}(\mathbf{Q}_h\mathbf{u}), \nabla_{w,d}\mathbf{v}\big)_E = (\mathbb{Q}_h\nabla\mathbf{u}, \nabla_{w,d}\mathbf{v})_E = \big\langle(\mathbb{Q}_h\nabla\mathbf{u})\mathbf{n}, \mathbf{v}^\partial - \mathbf{v}^\circ\big\rangle_{E^\partial},$$

and

$$\big(\nabla_{w,d}\cdot(\mathbf{Q}_h\mathbf{u}), \nabla_{w,d}\cdot\mathbf{v}\big)_E = (Q_h(\nabla\cdot\mathbf{u}), \nabla_{w,d}\cdot\mathbf{v})_E = \big\langle Q_h(\nabla\cdot\mathbf{u})\mathbf{n}, \mathbf{v}^\partial - \mathbf{v}^\circ\big\rangle_{E^\partial}.$$

Thus we have, by summing over the entire mesh,

$$\begin{aligned}\mathcal{A}_h^{GD}(\mathbf{Q}_h\mathbf{u}, \mathbf{v}) &= \mu\sum_{E\in\mathcal{E}_h}\big\langle(\mathbb{Q}_h\nabla\mathbf{u})\mathbf{n}, \mathbf{v}^\partial - \mathbf{v}^\circ\big\rangle_{E^\partial} \\ &\quad + (\mu+\lambda)\sum_{E\in\mathcal{E}_h}\big\langle Q_h(\nabla\cdot\mathbf{u})\mathbf{n}, \mathbf{v}^\partial - \mathbf{v}^\circ\big\rangle_{E^\partial}.\end{aligned} \tag{31}$$

Subtracting (31) from (30) yields the error equation claimed in (25). □

Lemma 7 (Estimates on linear functionals). *Assume the exact solution of* (4) *has regularity* $\mathbf{u} \in \mathbf{H}^2(\Omega)$. *Then for any* $\mathbf{v} \in V_h$, *there hold*

$$|\mathcal{G}_1(\mathbf{u}, \mathbf{v})| \lesssim h\|\mathbf{u}\|_{\mathbf{H}^2(\Omega)}|\|\mathbf{v}\||, \tag{32}$$

$$|\mathcal{G}_2(\mathbf{u}, \mathbf{v})| \lesssim h\|\nabla\cdot\mathbf{u}\|_{H^1(\Omega)}|\|\mathbf{v}\||. \tag{33}$$

Remarks If $\mathbf{u}$ is the exact solution of (4), then $\mathcal{G}_2(\mathbf{u}, \mathbf{v})$ and $\mathcal{G}_2(\mathbf{u}, \mathbf{v})$ are indeed linear functionals defined on V_h. In general, they can also be viewed as nonsymmetric bilinear forms defined on $\mathbf{H}^1(\Omega) \times V_h$. This will allow us to readily apply the above estimates in a duality argument to be presented later.

Proof Consider a fixed $E \in \mathcal{E}_h$. By Lemma 3 (trace equivalence) and the approximation capacity of $\mathbb{Q}_h$, we have

$$\|(\nabla \mathbf{u} - \mathbb{Q}_h \nabla \mathbf{u})\mathbf{n}\|_{E^\partial} \lesssim h_E^{-\frac{1}{2}} \|\nabla \mathbf{u} - \mathbb{Q}_h \nabla \mathbf{u}\|_E \lesssim h_E^{\frac{1}{2}} \|\mathbf{u}\|_{\mathbf{H}^2(E)}.$$

Applying the Cauchy–Schwarz and Young's inequalities, and the definition of semi-norm (18) gives

$$\begin{aligned} |\mathcal{G}_1(\mathbf{u}, \mathbf{v})| &\lesssim \left(\sum_{E \in \mathcal{E}_h} h_E \|(\nabla \mathbf{u} - \mathbb{Q}_h \nabla \mathbf{u})\mathbf{n}\|_E^2 \right)^{\frac{1}{2}} \left(\sum_{E \in \mathcal{E}_h} h_E^{-1} \|\mathbf{v}^\partial - \mathbf{v}^\circ\|_E^2 \right)^{\frac{1}{2}} \\ &\lesssim \left(\sum_{E \in \mathcal{E}_h} h_E^2 \|\mathbf{u}\|_{\mathbf{H}(E)}^2 \right)^{\frac{1}{2}} \left(\sum_{E \in \mathcal{E}_h} h_E^{-1} \|\mathbf{v}^\partial - \mathbf{v}^\circ\|_E^2 \right)^{\frac{1}{2}} \\ &\leq Ch \|\mathbf{u}\|_{\mathbf{H}^2(\Omega)} |||\mathbf{v}|||, \end{aligned} \tag{34}$$

as desired. The second estimate can be proven in a similar way. □

Theorem 1 *Let* $\mathbf{u}$ *be the exact solution of* (4) *and* $\mathbf{u}_h$ *be the numerical solution obtained from* (14)*. There holds*

$$\mu \sum_{E \in \mathcal{E}_h} \|\nabla \mathbf{u} - \nabla_{w,d} \mathbf{u}_h\|_E^2 + (\mu + \lambda) \sum_{E \in \mathcal{E}_h} \|\nabla \cdot \mathbf{u} - \nabla_{w,d} \cdot \mathbf{u}_h\|_E^2 \lesssim h^2 \|\mathbf{f}\|_{\mathbf{L}^2(\Omega)}^2. \tag{35}$$

Proof We utilize Lemma 1 (commuting identities) to split the elementwise errors into projection errors and discretization errors as shown below,

$$\begin{aligned} \|\nabla \mathbf{u} - \nabla_{w,d} \mathbf{u}_h\|_E^2 &\lesssim \|\nabla \mathbf{u} - \mathbb{Q}_h \nabla \mathbf{u}\|_E^2 + \|\mathbb{Q}_h \nabla \mathbf{u} - \nabla_{w,d} \mathbf{u}_h\|_E^2, \\ \|\nabla \cdot \mathbf{u} - \nabla_{w,d} \cdot \mathbf{u}_h\|_E^2 &\lesssim \|\nabla \cdot \mathbf{u} - Q_h(\nabla \cdot \mathbf{u})\|_E^2 + \|Q_h(\nabla \cdot \mathbf{u}) - \nabla_{w,d} \cdot \mathbf{u}_h\|_E^2. \end{aligned}$$

For the projection errors, we have first elementwise estimates

$$\begin{aligned} \|\nabla \mathbf{u} - \mathbb{Q}_h \nabla \mathbf{u}\|_E &\lesssim h \|\mathbf{u}\|_{\mathbf{H}^2(E)}, \\ \|\nabla \cdot \mathbf{u} - Q_h(\nabla \cdot \mathbf{u})\|_E &\lesssim h \|\nabla \cdot \mathbf{u}\|_{H^1(E)}, \end{aligned}$$

and then a mesh-wise estimate

$$\begin{aligned} &\mu \sum_{E \in \mathcal{E}_h} \|\nabla \mathbf{u} - \mathbf{Q_h} \nabla \mathbf{u}\|_E^2 + (\mu + \lambda) \sum_{E \in \mathcal{E}_h} \|\nabla \cdot \mathbf{u} - Q_h(\nabla \cdot \mathbf{u})\|_E^2 \\ &\lesssim h^2 \left(\mu \|\mathbf{u}\|_{\mathbf{H^2}(\Omega)}^2 + (\mu + \lambda) \|\nabla \cdot \mathbf{u}\|_{H^1(\Omega)}^2 \right) \lesssim h^2 \|\mathbf{f}\|_{\mathbf{L}^2(\Omega)}^2. \end{aligned} \tag{36}$$

In the last step, we have used the fact that

$$\mu \|\mathbf{u}\|_{\mathbf{H^2}(\Omega)}^2 + (\mu + \lambda) \|\nabla \cdot \mathbf{u}\|_{H^1(\Omega)}^2 \lesssim \|\mathbf{f}\|_{\mathbf{L}^2(\Omega)}^2,$$

which can be derived from (6) using the techniques developed in [4].

For the discretization errors between the projection and the finite element solution, we combine Lemmas 6 and 7 to obtain

$$\begin{aligned} &\mu \sum_{E \in \mathcal{E}_h} \|\mathbb{Q}_h \nabla \mathbf{u} - \nabla_{w,d} \mathbf{u}_h\|_E^2 + (\mu + \lambda) \sum_{E \in \mathcal{E}_h} \|Q_h(\nabla \cdot \mathbf{u}) - \nabla_{w,d} \cdot \mathbf{u}_h\|_E^2, \\ &\lesssim h^2 \left(\mu \|\mathbf{u}\|_{\mathbf{H^2}(\Omega)}^2 + (\mu + \lambda) \|\nabla \cdot \mathbf{u}\|_{H^1(\Omega)}^2 \right) \lesssim h^2 \|\mathbf{f}\|_{\mathbf{L}^2(\Omega)}^2. \end{aligned} \tag{37}$$

The desired result follows from combining (36) and (37). □

We now establish an L^2-norm estimate using a standard duality argument.

Theorem 2 (L^2-norm estimate for displacement). *Let* $\mathbf{u}$ *be the exact solution of* (4) *and* $\mathbf{u}_h$ *be the numerical solution obtained from* (14)*. There holds*

$$\|\mathbf{u} - \mathbf{u}_h^\circ\|_{L^2(\Omega)} \leq Ch\|\mathbf{f}\|_{\mathbf{L}^2(\Omega)}, \tag{38}$$

where C *is a positive constant independent of* λ, h.

Proof Let $\boldsymbol{\Phi}$ be the solution of the dual problem

$$\begin{cases} -\mu\Delta\boldsymbol{\Phi} - (\mu+\lambda)\nabla(\nabla\cdot\boldsymbol{\Phi}) = \mathbf{e}_h^\circ, \\ \boldsymbol{\Phi}|_{\partial\Omega} = \mathbf{0}. \end{cases} \tag{39}$$

As usual, we assume the dual solution has full regularity as follows

$$\mu\|\boldsymbol{\Phi}\|_{\mathbf{H}^2(\Omega)} + (\mu+\lambda)\|\nabla\cdot\boldsymbol{\Phi}\|_{H^1(\Omega)} \leq C\|\mathbf{e}_h^\circ\|_{\mathbf{L}^2(\Omega)}. \tag{40}$$

We test the dual equation against $\mathbf{v} \in V_h$ on an arbitrary element $E \in \mathcal{E}_h$ and apply integrating by parts to obtain

$$-\mu\langle(\nabla\boldsymbol{\Phi})\mathbf{n}, \mathbf{v}^\circ\rangle_{E^\partial} - (\mu+\lambda)\langle(\nabla\cdot\boldsymbol{\Phi})\mathbf{n}, \mathbf{v}^\circ\rangle_{E^\partial} = (\mathbf{e}_h^\circ, \mathbf{v}^\circ)_E. \tag{41}$$

The normal continuity and boundary conditions of the dual solution together imply

$$\sum_{E\in\mathcal{E}_h}\big\langle(\nabla\boldsymbol{\Phi})\mathbf{n}, \mathbf{v}^\partial\big\rangle_{E^\partial} = 0, \qquad \sum_{E\in\mathcal{E}_h}\big\langle(\nabla\cdot\boldsymbol{\Phi})\mathbf{n}, \mathbf{v}^\partial\big\rangle_{E^\partial} = 0. \tag{42}$$

Combined these yield

$$\sum_{E\in\mathcal{E}_h}(\mathbf{e}_h^\circ, \mathbf{v}^\circ)_E = \mu\sum_{E\in\mathcal{E}_h}\big\langle(\nabla\boldsymbol{\Phi})\mathbf{n}, \mathbf{v}^\partial - \mathbf{v}^\circ\big\rangle_{E^\partial} + (\mu+\lambda)\sum_{E\in\mathcal{E}_h}\big\langle(\nabla\cdot\boldsymbol{\Phi})\mathbf{n}, \mathbf{v}^\partial - \mathbf{v}^\circ\big\rangle_{E^\partial}. \tag{43}$$

Alternatively, applying Lemmas 1 (commuting identities) and 2 (conversion-to-trace formulas), we have elementwise

$$\begin{aligned} &\mu(\nabla_{w,d}(\mathbf{Q}_h\boldsymbol{\Phi}), \nabla_{w,d}\mathbf{v})_E + (\mu+\lambda)(\nabla_{w,d}\cdot(\mathbf{Q}_h\boldsymbol{\Phi}), \nabla_{w,d}\cdot\mathbf{v})_E \\ &= \mu(\mathbb{Q}_h\nabla\boldsymbol{\Phi}, \nabla_{w,d}\mathbf{v})_E + (\mu+\lambda)(Q_h(\nabla\cdot\boldsymbol{\Phi}), \nabla_{w,d}\cdot\mathbf{v})_E \\ &= \mu\big\langle(\mathbb{Q}_h\nabla\boldsymbol{\Phi})\mathbf{n}, \mathbf{v}^\partial - \mathbf{v}^\circ\big\rangle_{E^\partial} + (\mu+\lambda)\big\langle Q_h(\nabla\cdot\boldsymbol{\Phi})\mathbf{n}, \mathbf{v}^\partial - \mathbf{v}^\circ\big\rangle_{E^\partial}. \end{aligned}$$

Over the entire mesh, we have

$$\begin{aligned} \mathcal{A}_h^{GD}(\mathbf{Q}_h\boldsymbol{\Phi}, \mathbf{v}) = \mu&\sum_{E\in\mathcal{E}_h}\big\langle(\mathbb{Q}_h\nabla\boldsymbol{\Phi})\mathbf{n}, \mathbf{v}^\partial - \mathbf{v}^\circ\big\rangle_{E^\partial} \\ &+ (\mu+\lambda)\sum_{E\in\mathcal{E}_h}\big\langle Q_h(\nabla\cdot\boldsymbol{\Phi})\mathbf{n}, \mathbf{v}^\partial - \mathbf{v}^\circ\big\rangle_{E^\partial}. \end{aligned} \tag{44}$$

We now set $\mathbf{v} = \mathbf{e}_h$ in both (43) and (44), and perform a subtraction on both sides to obtain

$$\|\mathbf{e}_h^\circ\|^2 - \mathcal{A}_h^{GD}(\mathbf{Q}_h\boldsymbol{\Phi}, \mathbf{e}_h) = \mu\,\mathcal{G}_1(\boldsymbol{\Phi}, \mathbf{e}_h) + (\mu+\lambda)\,\mathcal{G}_2(\boldsymbol{\Phi}, \mathbf{e}_h).$$

The symmetry in $\mathcal{A}_h^{GD}(\cdot,\cdot)$ leads to

$$\|\mathbf{e}_h^\circ\|^2 = \mathcal{A}_h^{GD}(\mathbf{e}_h, \mathbf{Q}_h\boldsymbol{\Phi}) + \mu\,\mathcal{G}_1(\boldsymbol{\Phi}, \mathbf{e}_h) + (\mu+\lambda)\,\mathcal{G}_2(\boldsymbol{\Phi}, \mathbf{e}_h). \tag{45}$$

Similar to Lemma 7, we have immediately

$$|\mathcal{G}_1(\mathbf{\Phi}, \mathbf{e}_h)| \leq Ch\|\mathbf{\Phi}\|_{\mathbf{H}^2(\Omega)}|\|\mathbf{e}_h\||,$$
$$|\mathcal{G}_2(\mathbf{\Phi}, \mathbf{e}_h)| \leq Ch\|\nabla \cdot \mathbf{\Phi}\|_{H^1(\Omega)}|\|\mathbf{e}_h\||.$$

The above two estimates combined with the dual regularity (40) imply

$$|\mu\, \mathcal{G}_1(\mathbf{\Phi}, \mathbf{e}_h) + (\mu + \lambda)\, \mathcal{G}_2(\mathbf{\Phi}, \mathbf{e}_h)| \leq Ch\|\mathbf{e}_h^\circ\|\, |\|\mathbf{e}_h\||. \tag{46}$$

To estimate $|\|\mathbf{e}_h\||$, we first set $\mathbf{v} = \mathbf{e}_h$ in (25) and then apply Lemmas 4 (coercivity), 6, and 7 to obtain

$$|\|\mathbf{e}_h\|| \leq Ch\|\mathbf{f}\|_{\mathbf{L}^2(\Omega)}, \tag{47}$$

where $C > 0$ is a constant independent of h and λ.

Applying Lemmas 6 (error equation) and 7, and the regularity of the exact solution (6) yields

$$|\mathcal{A}_h^{GD}(\mathbf{e}_h, \mathbf{Q}_h\mathbf{\Phi})| \leq Ch\|\mathbf{f}\|_{\mathbf{L}^2(\Omega)}|\|\mathbf{Q}_h\mathbf{\Phi}\||.$$

Applying Lemmas 4 (coercivity) and 1(i) (commuting identity), the stability of the projection $\mathbf{Q}_h$ and dual regularity, we have

$$|\|\mathbf{Q}_h\mathbf{\Phi}\|| \lesssim \|\nabla_{w,d}(\mathbf{Q}_h\mathbf{\Phi})\| = \|\mathbb{Q}_h\nabla\mathbf{\Phi}\| \leq \|\nabla\mathbf{\Phi}\| \leq \|\mathbf{\Phi}\|_{\mathbf{H}^2(\Omega)} \lesssim \|\mathbf{e}_h^\circ\|.$$

Combining the above two estimates gives

$$\left|\mathcal{A}_h^{GD}(\mathbf{e}_h, \mathbf{Q}_h\mathbf{\Phi})\right| \leq Ch\|\mathbf{f}\|_{\mathbf{L}^2(\Omega)}\|\mathbf{e}_h^\circ\|. \tag{48}$$

Finally, combining (45), (46), (47), and (48) yields the desired result. □

Theorems 1 and 2 combined imply that for elasticity problems on rectangular meshes, the lowest-order WG finite element scheme $(Q_0^2,\, Q_0^2;\, RT_{[0]}^2,\, Q_0)$ has the following two properties.

- First order convergence in displacement, stress, and dilation (given full regularity of the exact solution);
- The convergence order does not deteriorate as $\lambda \to \infty$, i.e, the method is locking-free.

It is observed (see Sect. 6, Example 2) that for elasticity problems with low regularity, say, $\mathbf{u} \in \mathbf{H}^{1+s}(\Omega)$ with $s \in (0, 1)$, the method produces 1st order convergence in displacement and order s convergence in stress and dilation.

Remarks on the extension to quadrilateral and hexahedral meshes. It can be observed that the commuting identities in Lemma 1(i)(ii) play important roles in the error analysis. These identities demonstrate that the discrete weak gradient and the discrete weak divergence provide a good approximation to their classical counterparts.

Recall the definition of the discrete weak gradient,

$$\int_E (\nabla_{w,d}\mathbf{v}) : W = \int_{E^\partial} \mathbf{v}^\partial \cdot (W\mathbf{n}) - \int_{E^\circ} \mathbf{v}^\circ \cdot (\nabla \cdot W), \quad \forall W \in RT_{[0]}^2(E),$$

and Lemma 1(i)

$$\nabla_{w,d}(\mathbf{Q}_h\mathbf{u}) = \mathbb{Q}_h(\nabla\mathbf{u}).$$

The above two quantities are expected to be in the same finite dimensional space, say, the local Raviart–Thomas space $RT_{[0]}^2(E)$ on a rectangle E, from which we take a typical test

function W. By the definition of discrete weak gradient, the definition of the projection $\mathbf{Q}_h = \{\mathbf{Q}_h^\circ, \mathbf{Q}_h^\partial\}$, the definition of the projection $\mathbb{Q}_h$, and Gauss Divergence Theorem, we should have

$$\begin{aligned}
&\int_E \nabla_{w,d}(\mathbf{Q}_h\mathbf{u}) : W = \int_{E^\partial} \left(\mathbf{Q}_h^\partial \mathbf{u}\right) \cdot (W\mathbf{n}) - \int_{E^\circ} \left(\mathbf{Q}_h^\circ \mathbf{u}\right) \cdot (\nabla \cdot W) \\
&\quad \| \\
&\int_E \mathbb{Q}_h(\nabla \mathbf{u}) : W \\
&\quad \| \\
&\int_E (\nabla \mathbf{u}) : W = \int_{E^\partial} \mathbf{u} \cdot W\mathbf{n} - \int_{E^\circ} \mathbf{u} \cdot (\nabla \cdot W).
\end{aligned} \tag{49}$$

The 1st vertical equal sign holds due to the commuting property [Lemma 1(i)]. The 2nd vertical equal sign holds by the definition of the L^2-projection $\mathbb{Q}_h$. This leads to *Matching Condition I* for (8), namely

(i) $W\mathbf{n}$ (trace) lies in the same space as $\mathbf{v}^\partial$ or in a subspace of this space (applicable to $\mathbf{Q}_h^\partial \mathbf{u}$);
(ii) $\nabla \cdot W$ (div) lies in the same space as $\mathbf{v}^\circ$ or in a subspace of this space (applicable to $\mathbf{Q}_h^\circ \mathbf{u}$).

A similar analysis for Lemma 1(ii) leads to *Matching Condition II* for (10), namely

(i) The trace $w\mathbf{n}$ lies in the same space as $\mathbf{v}^\partial$ or in a subspace of this space;
(ii) The gradient ∇w lies in the same space as $\mathbf{v}^\circ$ or in a subspace of this space.

In this regard, for rectangles ($d = 2$) or bricks ($d = 3$), $(Q_0^d, Q_0^d; RT_{[0]}^d, Q_0)$ provide good combinations.

The commuting identities in Lemma 1(i)(ii) while elegant, are not necessary conditions. Generally speaking, if the discrepancy between each pair of quantities is a higher order quantity of the mesh size: $\mathcal{O}(h^{1+r})$ for some $r > 0$, then the error analysis in this section can still go through, although it will become more technically involved.

For the (Q_0^2, Q_0^2)-type discrete weak functions on quadrilaterals, there are two ways for constructing a space for their discrete weak gradients:

(i) Using the unmapped $RT_{[0]}^2$ space in this paper, for which the divergence $\nabla \cdot W$ is a constant vector, but the trace $W\mathbf{n}$ is not a constant vector;
(ii) Using the mapped $RT_{[0]}^2$ space based on the Piola transform, for which $W\mathbf{n}$ (trace) is a constant vector, but $\nabla \cdot W$ (div) is not a constant vector [6].

A similar discussion applies to hexahedra. When the quadrilaterals are asymptotically parallelogram or the hexahedra are asymptotically parallelepiped, the aforementioned discrepancy will be a higher order quantity of the mesh size. Thus our finite element schemes can be extended to these types of quadrilateral and hexahedral meshes, see Sect. 6, Examples 3 and 5 for numerical results.

4 Implementation

We have implemented WG$(Q_0^2, Q_0^2; RT_{[0]}^2, Q_0)$ on quadrilateral meshes (including rectangular meshes as a special case) in our `Matlab` code package `DarcyLite`; and

WG(Q_0^3, Q_0^3; $RT_{[0]}^3$, Q_0) on hexahedral meshes (including brick meshes as a special case) in our code package `Darcy+`. For convenience, we use the normalized coordinates [14]

$$X = x - x_c, \quad Y = y - y_c, \quad Z = z - z_c,$$

since $\int_E X = 0$, $\int_E Y = 0$, $\int_E Z = 0$ on a rectangle or brick E.

4.1 Calculation of Numerical Stress on a Quadrilateral

Recall the eight basis functions $W_j (1 \le j \le 8)$ defined in (7). We also need their averages

$$\overline{W}_j = \frac{1}{2}(W_j + W_j^T)$$

for strain and stress calculations. Specifically, we have

$$\begin{aligned} &\overline{W}_1 = \begin{bmatrix} 1 & 0 \\ 0 & 0 \end{bmatrix}, \ \overline{W}_2 = \begin{bmatrix} 0 & \frac{1}{2} \\ \frac{1}{2} & 0 \end{bmatrix}, \ \overline{W}_3 = \begin{bmatrix} X & 0 \\ 0 & 0 \end{bmatrix}, \ \overline{W}_4 = \begin{bmatrix} 0 & \frac{Y}{2} \\ \frac{Y}{2} & 0 \end{bmatrix}, \\ &\overline{W}_5 = \begin{bmatrix} 0 & \frac{1}{2} \\ \frac{1}{2} & 0 \end{bmatrix}, \ \overline{W}_6 = \begin{bmatrix} 0 & 0 \\ 0 & 1 \end{bmatrix}, \ \overline{W}_7 = \begin{bmatrix} 0 & \frac{X}{2} \\ \frac{X}{2} & 0 \end{bmatrix}, \ \overline{W}_8 = \begin{bmatrix} 0 & 0 \\ 0 & Y \end{bmatrix}. \end{aligned} \tag{50}$$

Let $\phi_i (1 \le i \le 10)$ be one of the ten WG(Q_0^2, Q_0^2) basis functions on a quadrilateral and its discrete weak gradient be

$$\nabla_{w,d}\phi_i = \sum_{j=1}^{8} c_{i,j} W_j, \quad 1 \le i \le 10.$$

Clearly, its discrete weak strain is

$$\varepsilon_{w,d}(\phi_i) = \sum_{j=1}^{8} c_{i,j} \overline{W}_j, \quad 1 \le i \le 10.$$

Its discrete weak divergence is just a constant,

$$\nabla_{w,d} \cdot \phi_i = d_i, \quad 1 \le i \le 10.$$

The definition for discrete weak stress gives

$$\sigma = 2\mu\, \varepsilon_{w,d}(\phi_i) + \lambda d_i\, \mathbb{I}_2, \qquad 1 \le i \le 10,$$

where $\mathbb{I}_2$ is the order 2 identity matrix. By direct calculations, we obtain the numerical stress corresponding to a single WG basis function $\phi_i (1 \le i \le 10)$ as

$$\begin{cases} \sigma_{xx} = \sigma_{11} = (2\mu c_{i,1} + \lambda d_i) + 2\mu c_{i,3} X, \\ \sigma_{yy} = \sigma_{22} = (2\mu c_{i,6} + \lambda d_i) + 2\mu c_{i,8} Y, \\ \sigma_{xy} = \sigma_{12} = \mu(c_{i,2} + c_{i,5}) + \mu c_{i,7} X + \mu c_{i,4} Y, \\ \sigma_{yx} = \sigma_{21} = \sigma_{12}. \end{cases} \tag{51}$$

This also states that the normal stress σ_{11} is a linear function of only the first coordinate, the normal stress σ_{22} is a linear function of only the second coordinate, whereas the shear stress σ_{12} is a linear function of both coordinates. In this regard, our numerical stress has the same form as that obtained from the simplest nonconforming finite element method investigated in [8].

For graphical results involving elementwise averages of the stress components, we use (51) and numerical integration.

4.2 Calculation of Numerical Stress on a Hexahedron

In the same spirit, we consider the eighteen normalized basis functions $W_j (1 \le j \le 18)$ for $RT^3_{[0]}$ on a hexahedron. Their averages are

$$
\begin{aligned}
&\overline{W}_1 = \begin{bmatrix} 1 & 0 & 0 \\ 0 & 0 & 0 \\ 0 & 0 & 0 \end{bmatrix}, \quad \overline{W}_2 = \begin{bmatrix} 0 & \frac{1}{2} & 0 \\ \frac{1}{2} & 0 & 0 \\ 0 & 0 & 0 \end{bmatrix}, \quad \overline{W}_3 = \begin{bmatrix} 0 & 0 & \frac{1}{2} \\ 0 & 0 & 0 \\ \frac{1}{2} & 0 & 0 \end{bmatrix}, \\
&\overline{W}_4 = \begin{bmatrix} X & 0 & 0 \\ 0 & 0 & 0 \\ 0 & 0 & 0 \end{bmatrix}, \quad \overline{W}_5 = \begin{bmatrix} 0 & \frac{Y}{2} & 0 \\ \frac{Y}{2} & 0 & 0 \\ 0 & 0 & 0 \end{bmatrix}, \quad \overline{W}_6 = \begin{bmatrix} 0 & 0 & \frac{Z}{2} \\ 0 & 0 & 0 \\ \frac{Z}{2} & 0 & 0 \end{bmatrix}, \\
&\overline{W}_7 = \begin{bmatrix} 0 & \frac{1}{2} & 0 \\ \frac{1}{2} & 0 & 0 \\ 0 & 0 & 0 \end{bmatrix}, \quad \overline{W}_8 = \begin{bmatrix} 0 & 0 & 0 \\ 0 & 1 & 0 \\ 0 & 0 & 0 \end{bmatrix}, \quad \overline{W}_9 = \begin{bmatrix} 0 & 0 & 0 \\ 0 & 0 & \frac{1}{2} \\ 0 & \frac{1}{2} & 0 \end{bmatrix}, \\
&\overline{W}_{10} = \begin{bmatrix} 0 & \frac{X}{2} & 0 \\ \frac{X}{2} & 0 & 0 \\ 0 & 0 & 0 \end{bmatrix}, \quad \overline{W}_{11} = \begin{bmatrix} 0 & 0 & 0 \\ 0 & Y & 0 \\ 0 & 0 & 0 \end{bmatrix}, \quad \overline{W}_{12} = \begin{bmatrix} 0 & 0 & 0 \\ 0 & 0 & \frac{Z}{2} \\ 0 & \frac{Z}{2} & 0 \end{bmatrix}, \\
&\overline{W}_{13} = \begin{bmatrix} 0 & 0 & \frac{1}{2} \\ 0 & 0 & 0 \\ \frac{1}{2} & 0 & 0 \end{bmatrix}, \quad \overline{W}_{14} = \begin{bmatrix} 0 & 0 & 0 \\ 0 & 0 & \frac{1}{2} \\ 0 & \frac{1}{2} & 0 \end{bmatrix}, \quad \overline{W}_{15} = \begin{bmatrix} 0 & 0 & 0 \\ 0 & 0 & 0 \\ 0 & 0 & 1 \end{bmatrix}, \\
&\overline{W}_{16} = \begin{bmatrix} 0 & 0 & \frac{X}{2} \\ 0 & 0 & 0 \\ \frac{X}{2} & 0 & 0 \end{bmatrix}, \quad \overline{W}_{17} = \begin{bmatrix} 0 & 0 & 0 \\ 0 & 0 & \frac{Y}{2} \\ 0 & \frac{Y}{2} & 0 \end{bmatrix}, \quad \overline{W}_{18} = \begin{bmatrix} 0 & 0 & 0 \\ 0 & 0 & 0 \\ 0 & 0 & Z \end{bmatrix}.
\end{aligned} \tag{52}
$$

Similarly, let $\phi_i (1 \le i \le 21)$ be a $\mathrm{WG}(Q_0^3, Q_0^3)$ basis function. Assume its discrete weak gradient and discrete weak divergence are respectively

$$
\nabla_{w,d}\phi_i = \sum_{j=1}^{18} c_{i,j} W_j, \qquad \nabla_{w,d} \cdot \phi_i = d_i, \qquad 1 \le i \le 21.
$$

Then its discrete weak stress is

$$
\sigma_{w,d}(\phi_i) = 2\mu \sum_{j=1}^{18} c_{i,j} \overline{W}_j + \lambda d_i \mathbb{I}_3, \quad 1 \le i \le 21.
$$

The components of the stress tensor are (see [8] also)

$$
\begin{cases}
\sigma_{xx} = (2\mu c_{i,1} + \lambda d_i) + 2\mu c_{i,4} X, \\
\sigma_{yy} = (2\mu c_{i,8} + \lambda d_i) + 2\mu c_{i,11} Y, \\
\sigma_{zz} = (2\mu c_{i,15} + \lambda d_i) + 2\mu c_{i,18} Z, \\
\sigma_{xy} = \mu(c_{i,2} + c_{i,7}) + \mu c_{i,10} X + \mu c_{i,5} Y, \\
\sigma_{xz} = \mu(c_{i,3} + c_{i,13}) + \mu c_{i,16} X + \mu c_{i,6} Z, \\
\sigma_{yz} = \mu(c_{i,9} + c_{i,14}) + \mu c_{i,17} Y + \mu c_{i,12} Z.
\end{cases} \tag{53}
$$

4.3 Block Diagonal Schur Complement

A salient feature of WGFEMs is the non-interaction between the basis functions defined in the interiors of different elements in the mesh. This motivates the use of Schur complement when solving the discrete linear system resulting from (11) or (14).

For ease of presentation, we assume the aforementioned linear system is partitioned as follows

$$\begin{bmatrix} \mathbf{A}_{00} & \mathbf{A}_{01} \\ \mathbf{A}_{10} & \mathbf{A}_{11} \end{bmatrix} \begin{bmatrix} \mathbf{x}_0 \\ \mathbf{x}_1 \end{bmatrix} = \begin{bmatrix} \mathbf{b}_0 \\ \mathbf{b}_1 \end{bmatrix}, \tag{54}$$

where label 0 refers to the degrees of freedom (DOFs) in element interiors, and label 1 refers to the DOFs on element interfaces.

The first equation

$$\mathbf{A}_{00}\mathbf{x}_0 + \mathbf{A}_{01}\mathbf{x}_1 = \mathbf{b}_0$$

can be easily solved as

$$\mathbf{x}_0 = \mathbf{A}_{00}^{-1}\left(\mathbf{b}_0 - \mathbf{A}_{01}\mathbf{x}_1\right), \tag{55}$$

based on the assumption that $\mathbf{A}_{00}$ is invertible and $\mathbf{x}_1$ is available.

Substituting the above solution into the 2nd equation in (54) produces

$$\left(\mathbf{A}_{11} - \mathbf{A}_{10}\mathbf{A}_{00}^{-1}\mathbf{A}_{01}\right)\mathbf{x}_1 = \mathbf{b}_1 - \mathbf{A}_{10}\mathbf{A}_{00}^{-1}\mathbf{b}_0, \tag{56}$$

which concerns only the unknown $\mathbf{x}_1$ and has a smaller size than the original linear system. Here $\widehat{\mathbf{A}_{11}} = \mathbf{A}_{11} - \mathbf{A}_{10}\mathbf{A}_{00}^{-1}\mathbf{A}_{01}$ is called the Schur complement (matrix) of the original partitioned coefficient matrix in (54).

Usually, the Schur complement matrix is not formed explicitly, since it can be expensive to compute. An iterative solver for (56) mainly requires the matrix-vector multiplication

$$\widehat{\mathbf{A}_{11}}\,\mathbf{v} = \mathbf{A}_{11}\mathbf{v} - \mathbf{A}_{10}\mathbf{A}_{00}^{-1}\mathbf{A}_{01}\mathbf{v}.$$

This corresponds to four matrix-vector multiplications and one vector subtraction. For WGFEMs, $\mathbf{A}_{00}$ is a block diagonal matrix where each block is a small-size SPD matrix, hence $\mathbf{A}_{00}^{-1}$ can be pre-computed. For an elasticity problem using the lowest-order weak Galerkin method (Q_0^3, Q_0^3; $RT_{[0]}^3$, Q_0) on a brick or hexahedral mesh, $\mathbf{A}_{00}$ is a block diagonal matrix where each block is a 3×3 SPD matrix. Its inverse can be obtained using Cholesky factorization.

5 A Related Method: WG(P_1^2, P_{rm}; $P_0^{2\times 2}$, P_0) with Stabilization

In [18], a family of WG finite element schemes were developed for general polygonal and polyhedral meshes, from which we can derive a particular WG method on rectangular meshes: WG(P_1^2, P_{rm}; $P_0^{2\times 2}$, P_0). Here P_1^2 means linear vector polynomials are used for element interiors, and P_{rm} means the edgewise space of rigid motions is used. Note that $\dim(P_{rm}) = 3$. Elementwise there are 18 degrees of freedom for each rectangle. For these WG basis functions, however, their discrete weak gradients are just constant 2×2 matrices, and their discrete weak divergences are also constants.

Here is a brief list of comparison. Our method:

– Does not require stabilization;

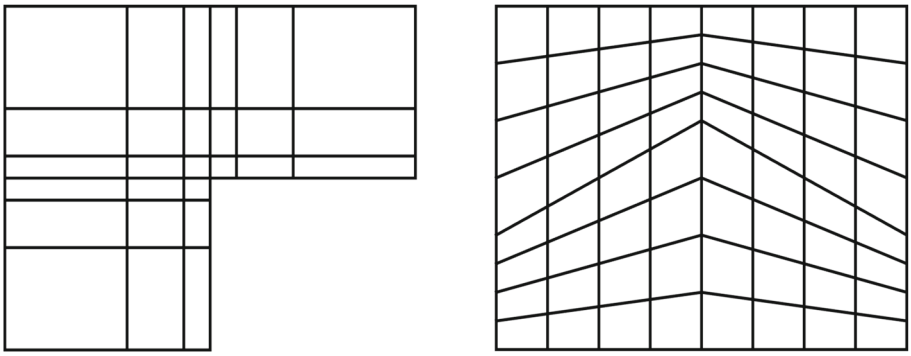

Fig. 1 Some meshes used in numerical experiments: Left: An initial graded mesh used in Example 2 Case II; Right: An initial trapezoidal meshed used in Example 3 (see [3] also)

– Uses fewer degrees of freedom;
– Achieves first-order convergence in displacement, stress, and dilation.

The WG(P_1^2, P_{rm}; $P_0^{2\times 2}$, P_0) method derived from [18] has the following properties:

– Requires stabilization;
– Has 2nd order convergence in displacement but only 1st order in stress and dilation;
– Can be applied to more general polygonal meshes.

6 Numerical Experiments

In this section we present numerical experiments for the new WG solvers for linear elasticity on rectangular and brick meshes. We include also numerical results on asymptotically parallelogram quadrilateral (parallelepiped hexahedral) meshes. We observe the expected locking-free property and optimal order convergence in displacement, stress, and dilation. The performance of the computational approach using the Schur complement is also examined. In addition to uniform rectangular and brick meshes, we use also graded rectangular meshes and asymptotically parallelogram trapezoidal meshes (Fig. 1).

Example 1 (*Locking-free*). This example is a variant of Example 1 in [7]. Specifically, the domain is $\Omega = (0, 1)^2$, a Neumann condition is posed on the right boundary of the domain, whereas the other three sides have Dirichlet conditions. The known exact solution for displacement is

$$\mathbf{u}(x, y) = \begin{bmatrix} (\pi/2)\sin^2(\pi x)\sin(2\pi y) \\ -(\pi/2)\sin(2\pi x)\sin^2(\pi y) \end{bmatrix} + \frac{1}{\lambda}\begin{bmatrix} \sin(\pi x)\sin(\pi y) \\ \sin(\pi x)\sin(\pi y) \end{bmatrix},$$

and hence

$$\nabla \cdot \mathbf{u} = \frac{\pi}{\lambda}\cos(\pi(x + y)) = \frac{(1 + \nu)(1 - 2\nu)}{E\nu}\pi\cos(\pi(x + y)).$$

It is clear that $\nabla \cdot \mathbf{u} \neq 0$ if $\nu \in (0, \frac{1}{2})$, and $\nabla \cdot \mathbf{u} = 0$ if $\nu = \frac{1}{2}$.

Numerical results for WG(Q_0^2, Q_0^2; $RT_{[0]}$, Q_0) on rectangular meshes are shown in Tables 1 and 2. The convergence rates in displacement, stress, and dilation are demonstrably first order for two different values of λ that are six orders of magnitude apart.

Table 1 Example 1: $\lambda = 1.6644 * 10^2$, WG(Q_0^2, Q_0^2; $RT_{[0]}$, Q_0) on rectangular meshes

$1/h$	$\|\mathbf{u} - \mathbf{u}_h^\circ\|$	$\|\sigma - \sigma_h\|$	$\|\nabla \cdot \mathbf{u} - \nabla_{w,d} \cdot \mathbf{u}_h\|$
8	2.5288E−1	6.6770E−1	2.1689E−3
16	1.2609E−1	3.2291E−1	1.0745E−3
32	6.2981E−2	1.6009E−1	5.3561E−4
64	3.1482E−2	8.0209E−2	2.6756E−4
Conv. rate	1st order	1st order	1st order

Table 2 Example 1: $\lambda = 1.667 * 10^8$, WG(Q_0^2, Q_0^2; $RT_{[0]}$, Q_0) on rectangular meshes

$1/h$	$\|\mathbf{u} - \mathbf{u}_h^\circ\|$	$\|\sigma - \sigma_h\|$	$\|\nabla \cdot \mathbf{u} - \nabla_{w,d} \cdot \mathbf{u}_h\|$
8	2.5289E−1	6.6702E−1	2.1665E−09
16	1.2609E−1	3.2245E−1	1.0731E−09
32	6.2981E−2	1.5967E−1	5.3491E−10
64	3.1482E−2	7.9625E−2	2.6721E−10
Conv. rate	1st order	1st order	1st order

Example 2 (*Low-regularity*). This example is derived from [1]. The problem is posed on a Γ-shaped domain $\Omega = (-1, 1)^2 \setminus ([0, 1] \times [-1, 0])$ with a body force $\mathbf{f} = \mathbf{0}$. The known analytical solution for displacement in polar coordinates is

$$\mathbf{u} = \Big[A\cos\theta - B\sin\theta,\ A\sin\theta + B\cos\theta\Big]^T =: [C, D]^T, \tag{57}$$

where (r, θ) are the polar coordinates and

$$\begin{cases} A = \dfrac{r^\alpha}{2\mu}\Big(-(1+\alpha)\cos((1+\alpha)\theta) + C_1(C_2 - 1 - \alpha)\cos((1-\alpha)\theta)\Big), \\ B = \dfrac{r^\alpha}{2\mu}\Big((1+\alpha)\sin((1+\alpha)\theta) - C_1(C_2 - 1 + \alpha)\sin((1-\alpha)\theta)\Big). \end{cases} \tag{58}$$

Here $\alpha \approx 0.544483737$ is the so-called *critical exponent*.

We present further details about the exact solution that were not provided in the original paper [1]. The dilation is

$$\nabla \cdot \mathbf{u} = \partial_r A + (\partial_\theta B)/r + A/r, \tag{59}$$

where

$$\begin{cases} \partial_r A = A\dfrac{\alpha}{r}, \qquad \partial_r B = B\dfrac{\alpha}{r}, \\ \partial_\theta A = \dfrac{r^\alpha}{2\mu}\Big((1+\alpha)^2\sin((1+\alpha)\theta) - C_1(C_2 - 1 - \alpha)(1-\alpha)\sin((1-\alpha)\theta)\Big), \\ \partial_\theta B = \dfrac{1}{2\mu}r^\alpha\Big((1+\alpha)^2\cos((1+\alpha)\theta) - C_1(C_2 - 1 + \alpha)(1-\alpha)\cos((1-\alpha)\theta)\Big). \end{cases} \tag{60}$$

The stress is

$$\sigma = \begin{bmatrix} 2\mu(\partial_x C) + \lambda(\nabla \cdot \mathbf{u}) & \mu(\partial_y C + \partial_x D) \\ \mu(\partial_y C + \partial_x D) & 2\mu(\partial_y D) + \lambda(\nabla \cdot \mathbf{u}) \end{bmatrix}, \tag{61}$$

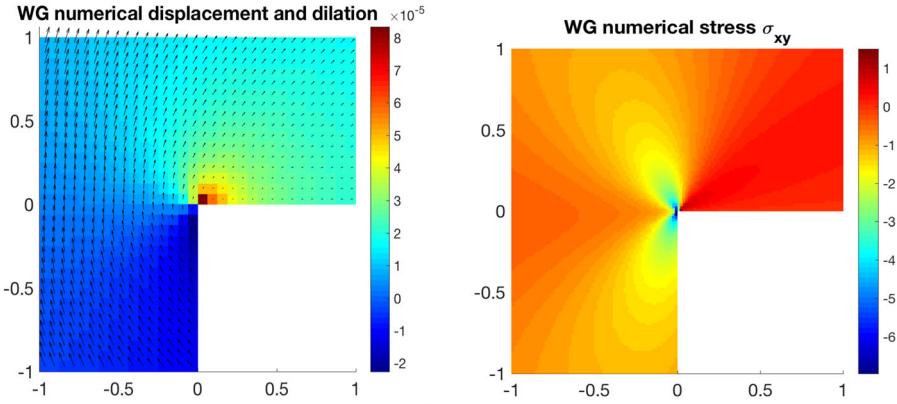

Numerical displacement and dilation for $h = \frac{1}{16}$ Numerical shear stress σ_{xy} for $h = \frac{1}{64}$

Fig. 2 Example 2 Case I ($\nu = 0.3$): Low-regularity captured by the lowest-order WG method on rectangular meshes

where

$$\begin{cases} \partial_x C = (\partial_r A)\cos^2\theta - (\partial_\theta A)\dfrac{\cos\theta\sin\theta}{r} + A\dfrac{\sin^2\theta}{r} \\ \qquad - (\partial_r B)\cos\theta\sin\theta + (\partial_\theta B)\dfrac{\sin^2\theta}{r} + B\dfrac{\cos\theta\sin\theta}{r}, \\ \partial_y D = (\partial_r A)\sin^2\theta + (\partial_\theta A)\dfrac{\cos\theta\sin\theta}{r} + A\dfrac{\cos^2\theta}{r} \\ \qquad + (\partial_r B)\cos\theta\sin\theta + (\partial_\theta B)\dfrac{\cos^2\theta}{r} - B\dfrac{\cos\theta\sin\theta}{r}, \\ \partial_y C + \partial_x D = (\partial_r A)\sin(2\theta) + (\partial_\theta A)\dfrac{\cos(2\theta)}{r} - A\dfrac{\sin(2\theta)}{r} \\ \qquad + (\partial_r B)\cos(2\theta) - (\partial_\theta B)\dfrac{\sin(2\theta)}{r} - B\dfrac{\cos(2\theta)}{r}. \end{cases} \tag{62}$$

We choose $E = 10^5$, $\nu = 0.3$ (Case I) or $\nu = 0.49999$ (Case II).

For Case I ($\nu = 0.3$), Table 3 shows the numerical results of the lowest-order WG(Q_0, Q_0; $RT^2_{[0]}$, Q_0) method applied to a family of rectangular meshes. The displacement error has first order convergence, whereas the stress and dilation errors have convergence

Table 3 Example 2 Case I ($\nu = 0.3$): lowest-order WG on uniform rectangular meshes

$1/h$	$\|\mathbf{u} - \mathbf{u}_h^\circ\|$	$\|\sigma - \sigma_h\|$	$\|\nabla\cdot\mathbf{u} - \nabla_{w,d}\cdot\mathbf{u}_h\|$
8	3.5814E−6	7.4745E−1	4.0348E−6
16	1.7968E−6	5.1626E−1	2.7822E−6
32	8.9935E−7	3.5529E−1	1.9134E−6
64	4.4972E−7	2.4407E−1	1.3141E−6
128	2.2480E−7	1.6751E−1	9.0181E−7
Conv. rate	0.998	0.539	0.540

Table 4 Example 2 Case II ($\nu = 0.49999$): lowest-order WG on graded rectangular meshes

Refinements	$\|\mathbf{u} - \mathbf{u}_h^\circ\|$	Rate	$\|\sigma - \sigma_h\|$	Rate	$\|\nabla \cdot \mathbf{u} - \nabla_{w,d} \cdot \mathbf{u}_h\|$	Rate
2	2.5254E−6	–	4.0880E−1	–	1.3870E−10	–
3	1.2630E−6	0.99	2.6754E−1	0.61	8.8424E−11	0.64
4	6.3149E−7	1.00	1.7960E−1	0.57	5.8522E−11	0.59
5	3.1571E−7	1.00	1.2189E−1	0.55	3.9426E−11	0.56
6	1.5784E−7	1.00	8.3149E−2	0.55	2.6792E−11	0.55

rates of approximately 0.54, close to the critical exponent α. The singularity at the origin is also clearly reflected in the profiles of the numerical dilation and stress shown in Fig. 2.

For Case II ($\nu = 0.49999$), we utilize graded meshes [13]. An initial mesh is shown in Fig. 1 left panel, which has three partitions for the boundary segments connecting $(0, 0)$ to $(1, 0)$ or $(0, 0)$ to $(0, -1)$. Successive regular refinements are performed. The results in Table 4 indicate that our WG method handles the dual challenges of a corner singularity and near-incompressibility very well, since the convergence rates for displacement, stress and dilation are essentially unchanged from the case when $\nu = 0.3$.

Example 3 For this example adopted from [8], the domain is $\Omega = (0, 1)^2$, and the Lamé constants are $\lambda = 1$ and $\mu = 0.5$. A homogeneous Dirichlet boundary condition is specified on the entire boundary. The known analytical solution for displacement is $\mathbf{u} = [4x(1 - x)y(1 - y), -4x(1 - x)y(1 - y)]^T$.

Numerical results using WG(Q_0^2, Q_0^2; $RT_{[0]}^2$, Q_0) on rectangular meshes and asymptotically parallelogram trapezoidal meshes adopted from [3] are shown in Table 5. These demonstrate first order convergence in displacement, stress, and dilation for both types of meshes.

Here we provide a concise definition for *asymptotically parallelogram* using element diameters and certain angles [3,15]. Let E be a quadrilateral, θ_1 be the angle between the outward unit normal vectors on two opposite edges, θ_2 be the angle for the other two edges. Let $\sigma_E = \max\{|\pi - \theta_1|, |\pi - \theta_2|\}$ and h_E be the diameter of E. A quadrilateral mesh $\mathcal{E}_h$ is *asymptotically parallelogram* [3], provided that there exists a positive constant C such that $\sigma_E / h_E \leq C$ for all $E \in \mathcal{E}_h$.

Clearly, quadrilateral or hexahedral meshes are more flexible than rectangular or brick meshes in accommodating complicated domain geometry. It is known that quality of quadrilateral or hexahedral meshes affects approximation accuracy [3]. In this regard, asymptotically parallelogram quadrilateral meshes or asymptotically parallelepiped hexahedral meshes meet the needs well. On one hand, any polygonal or polyhedral domain can be partitioned into such meshes [3]. On the other hand, our WG methods on such meshes provide satisfactory finite element solutions for linear elasticity, as shown by the above numerical results and the discussion near the end of Sect. 3.

Example 4 (Comparison with WG(P_1^2, P_{rm}; $P_0^{2\times 2}$, P_0) method) This example is directly taken from [18] p. 359 testcase 9.3. In particular, $\Omega = (0, 1)^2$, $\lambda = 1$, $\mu = 0.5$.

Numerical results for the WG(Q_0^2, Q_0^2; $RT_{[0]}^2$, Q_0) method developed in this paper and for the WG(P_1^2, P_{rm}; $P_0^{2\times 2}$, P_0) method with $\rho = 1$ derived from [18] are shown in Table 6 for a sequence of rectangular meshes. As expected, the lowest-order WG method derived in this paper exhibits first order convergence in displacement and stress. For the WG method

Table 5 Example 3: results of WG(Q_0^2, Q_0^2; $RT_{[0]}^2$, Q_0) on rectangular meshes and asymptotically parallelogram trapezoidal meshes adopted from [3]

	Rectangular meshes			Asymp. parallelogram trapezoidal meshes		
$1/h$	$\|\mathbf{u}-\mathbf{u}_h^\circ\|$	$\|\sigma-\sigma_h\|$	$\|\nabla\cdot\mathbf{u}-\nabla_{w,d}\cdot\mathbf{u}_h\|$	$\|\mathbf{u}-\mathbf{u}_h^\circ\|$	$\|\sigma-\sigma_h\|$	$\|\nabla\cdot\mathbf{u}-\nabla_{w,d}\cdot\mathbf{u}_h\|$
2^3	3.032E−2	1.547E−1	1.002E−1	3.106E−2	1.762E−1	1.046E−1
2^4	1.520E−2	7.752E−2	5.038E−2	1.556E−2	8.756E−2	5.248E−2
2^5	7.605E−3	3.878E−2	2.522E−2	7.784E−3	4.368E−2	2.625E−2
2^6	3.803E−3	1.939E−2	1.261E−2	3.892E−3	2.182E−2	1.312E−2
Rate	1st order	1st order	1st order	1st order	1st order	1st order

Table 6 Example 4: results of two WG methods on rectangular meshes

	WG (Q_0^2, Q_0^2; $RT_{[0]}^2$, Q_0)			WG (P_1^2, P_{rm}; $P_0^{2\times 2}$, P_0) with $\rho=1$		
$1/h$	$\|\mathbf{u}-\mathbf{u}_h^\circ\|$	$\|\sigma-\sigma_h\|$	$\|\nabla\cdot\mathbf{u}-\nabla_{w,d}\cdot\mathbf{u}_h\|$	$\|\mathbf{u}-\mathbf{u}_h^\circ\|$	$\|\sigma-\sigma_h\|$	$\|\nabla\cdot\mathbf{u}-\nabla_{w,d}\cdot\mathbf{u}_h\|$
2^3	6.029E−2	2.823E−2	1.104E−3	5.750E−3	4.489E−2	6.621E−3
2^4	3.015E−2	1.404E−2	3.132E−4	1.483E−3	2.082E−2	2.087E−3
2^5	1.507E−2	7.011E−3	8.648E−5	3.746E−4	1.007E−2	6.093E−4
2^6	7.538E−3	3.504E−3	2.347E−5	9.394E−5	4.980E−3	1.711E−4
Rate	1st order	1st order	≈ 1.85	2nd order	1st order	≈ 1.75

derived in [18], the displacement has 2nd order convergence, since linear polynomials are used for approximation. However, its stress has only 1st order convergence, since the discrete weak gradient is in $P_0^{2\times 2}$ and the discrete weak divergence is in P_0. For both WG methods, numerical dilation exhibit superconvergence. However, this phenomena is specific to this example and the theoretical convergence rates are just one.

Example 5 (*Schur complement*). For this 3-dim example, $\Omega = (0,1)^3$, $\lambda = \mu = 1$, the known exact solution for displacement is

$$\mathbf{u} = \frac{1}{3\pi}\begin{bmatrix} \sin(\pi x)\cos(\pi y)\cos(\pi z) \\ \cos(\pi x)\sin(\pi y)\cos(\pi z) \\ \cos(\pi x)\cos(\pi y)\sin(\pi z) \end{bmatrix}. \tag{63}$$

Accordingly, the dilation is

$$\nabla\cdot\mathbf{u} = \cos(\pi x)\cos(\pi y)\cos(\pi z). \tag{64}$$

The body force is $\mathbf{f} = 6\pi^2(\lambda+2\mu)\mathbf{u}$ and the exact stress is

$$\sigma = \begin{bmatrix} \sigma_{xx} & \sigma_{xy} & \sigma_{xz} \\ \sigma_{yx} & \sigma_{yy} & \sigma_{yz} \\ \sigma_{zx} & \sigma_{zy} & \sigma_{zz} \end{bmatrix},$$

where

$$\begin{cases} \sigma_{xx} = \sigma_{yy} = \sigma_{zz} = (3\lambda + 2\mu)/3 \cos(\pi x)\cos(\pi y)\cos(\pi z), \\ \sigma_{xy} = (-2\mu/3) \sin(\pi x)\sin(\pi y)\cos(\pi z), \\ \sigma_{xz} = (-2\mu/3) \sin(\pi x)\cos(\pi y)\sin(\pi z), \\ \sigma_{yz} = (-2\mu/3) \cos(\pi x)\sin(\pi y)\sin(\pi z). \end{cases} \tag{65}$$

This problem is solved using WG(Q_0^3, Q_0^3; $RT_{[0]}^3$, Q_0) on a sequence of hexahedral meshes adopted from [20], which are smooth perturbations of brick meshes. Specifically, the hexahedral mesh nodes are

$$\begin{cases} x = \hat{x} + 0.03 \sin(3\pi\hat{x})\cos(3\pi\hat{y})\cos(3\pi\hat{z}), \\ y = \hat{y} - 0.04 \cos(3\pi\hat{x})\sin(3\pi\hat{y})\cos(3\pi\hat{z}), \\ z = \hat{z} + 0.05 \sin(3\pi\hat{x})\cos(3\pi\hat{y})\sin(3\pi\hat{z}), \end{cases}$$

where $(\hat{x}, \hat{y}, \hat{z})$ are the brick mesh nodes. Both single-matrix and Schur-complement approaches are tested. As shown in Tables 7 and 8, the errors in displacement, stress, and dilation are the same, since two equivalent discrete linear systems are solved. However, it can be observed that the numbers of iterations for the Schur-complement approach are about half of those for the single-matrix approach.

Example 6 (*A nearly incompressible block under compression*). This example is taken from [17]. An elastic body has elasticity modulus $E = 240.56595979$ and Poisson's ratio $\nu = 0.499899987$, respectively. Accordingly, its Lamé constants are $\lambda = 4.00837688 * 10^5$ and $\mu = 8.0194 * 10^1$. This brick-shaped body is under compression on the middle part of its two opposite surfaces. Utilizing symmetry, we consider the top-upper-right octant of the

Table 7 Example 5: lowest-order WG solver on hexahedral meshes: single-matrix approach

$1/h$	$\|\mathbf{u} - \mathbf{u}_h^\circ\|$	$\|\sigma - \sigma_h\|$	$\|\nabla\cdot\mathbf{u} - \nabla_{w,d}\cdot\mathbf{u}_h\|$	DOFs	#Itr	Runtime (s)
4	2.488E−2	3.557E−1	1.361E−1	912	116	0.4
8	1.289E−2	1.875E−1	7.034E−2	6720	312	3.5
16	6.552E−3	9.564E−2	3.574E−2	51456	706	46
32	3.291E−3	4.795E−2	1.793E−2	402432	1415	610
64	1.648E−3	2.398E−2	8.968E−3	3182592	2748	8183
Rate	0.97	0.97	0.98			

Table 8 Example 5: lowest-order WG on hexahedral meshes: Schur-complement approach

$1/h$	$\|\mathbf{u} - \mathbf{u}_h^\circ\|$	$\|\sigma - \sigma_h\|$	$\|\nabla\cdot\mathbf{u} - \nabla_{w,d}\cdot\mathbf{u}_h\|$	DOFs	#Itr	Runtime (s)
4	2.488E−2	3.557E−1	1.361E−1	720	69	0.3
8	1.289E−2	1.875E−1	7.034E−2	5184	168	3.2
16	6.552E−3	9.564E−2	3.574E−2	39168	352	31
32	3.291E−3	4.795E−2	1.793E−2	304128	659	355
64	1.648E−3	2.398E−2	8.968E−3	2396160	1292	4608
Rate	0.97	0.97	0.98			

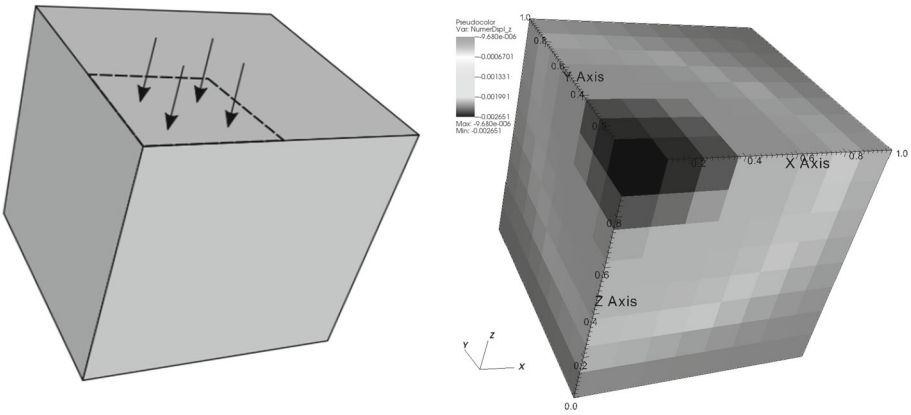

Fig. 3 Example 6: A nearly incompressible block under compression. Left: An illustration for the problem; Right: A profile of the vertical displacement (z-component) obtained from using WG(Q_0^3, Q_0^3; $RT_{[0]}^3$, Q_0) with $h = 1/8$

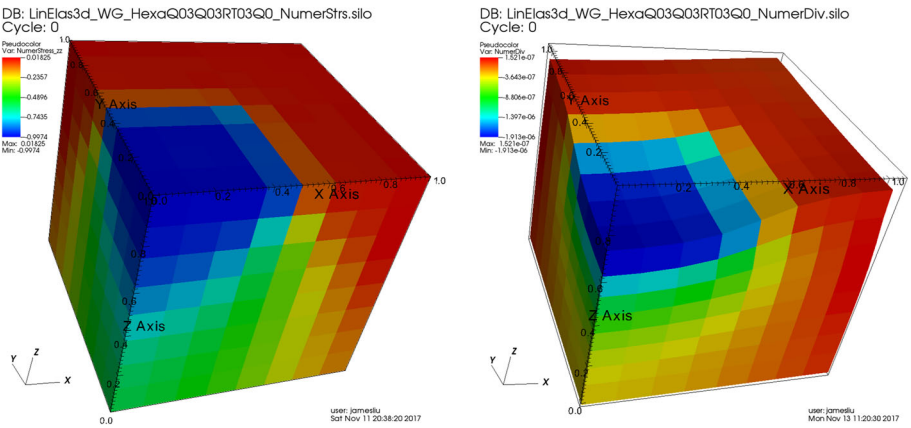

Fig. 4 Example 6: WG(Q_0^3, Q_0^3; $RT_{[0]}^3$, Q_0) applied with $h = 1/8$. Left: Profile of elementwise normal stress σ_{zz}; Right: Elementwise dilation (divergence of displacement) and deformation (magnified by 100 times). (Plots were produced using VisIt [12].)

brick domain and set the origin at the center to give an elasticity problem posed on the unit cube $\Omega = (0, 1)^3$, see Fig. 3 left panel. The symmetry implies that for the displacement $\mathbf{u} = [u_1, u_2, u_3]^T$, we have $u_1 = 0$ on the left face $x = 0$, $u_2 = 0$ on the back face $y = 0$, $u_3 = 0$ on the bottom face $z = 0$. A constant downward traction $[0, 0, -1]^T$ (point-wise) is posed on $(0, \frac{1}{2})^2 \times \{z = 1\}$. No analytical solution is available for this problem.

We apply the lowest-order WG(Q_0^3, Q_0^3; $RT_{[0]}^3$, Q_0) finite element method on a uniform $8 \times 8 \times 8$ brick mesh. The normal stress σ_{zz} is shown Fig. 4 left panel. The numerical dilation and deformation using the displacement values in element interiors is shown in the right panel of Fig. 4. The deformation was magnified by 100 times for better visual effect. It can be clearly observed that the external faces $\{x = 1\}$ and $\{y = 1\}$ are deformed inwards, while the top face (lower-left part) is being deformed downwards. The lowest-order weak Galerkin method is therefore able to capture the main features of this problem on even a very coarse mesh.

7 Concluding Remarks

In this paper we have investigated lowest-order weak Galerkin finite element methods for linear elasticity on rectangular and brick meshes. These new methods are locking-free, as demonstrated by theoretical analysis and numerical experiments. The new solvers produce first order accuracy in displacement, stress, and dilation when the problems have full regularity.

Our work is closely related to that in [8] in terms of seeking simplicity of the method. Here is a brief comparison. The method in [8]:

- is in the mixed formulation and results in a saddle-point problem;
- has fewer DOFs per element: 9 in 2-dim and 18 in 3-dim;
- is 1st order accurate in displacement and stress.

Our methods

- are in primal formulation for displacement, resulting in SPD linear systems;
- have slightly more DOFs per element: 10 in 2-dim and 21 in 3-dim;
- are 1st order accurate in displacement, stress, and dilation;
- are extendable to quadrilateral and hexahedral meshes.

Our methods apply to asymptotically parallelogram (parallelepiped) quadrilateral (hexahedral) meshes. This assumption on mesh quality is not really a severe restriction, since a polygonal domain can be partitioned into a family of asymptotically parallelogram quadrilateral meshes [3]. Similarly, a polyhedral domain can be partitioned into a family of asymptotically parallelepiped hexahedral meshes by nested refinement [23].

If general polygonal or polyhedral meshes need to be used, then the WG methods developed in [18] could be used, which involve penalization and at least linear polynomials inside elements.

We can also develop higher order ($k \geq 1$) WG(Q_k^d, Q_k^d; $RT_{[k]}^d$, Q_k) ($d = 2$ or 3) methods for linear elasticity on asymptotically parallelogram quadrilateral meshes or asymptotically parallelepiped hexahedral meshes. The main ideas are similar, but theoretical analysis and implementation will be more technically involved.

The lowest-order WG solvers for linear elasticity presented in this paper have been implemented in `Matlab` (for 2-dim) and C++ (for 3-dim). The source codes are respectively included in our software packages `DarcyLite` and `Darcy+`, which are freely available on the 2nd author's webpage. We plan to migrate our codes to `deal.II` platform so that these new solvers will be accessible to more researchers.

References

1. Alberty, J., Carstensen, C., Funken, S., Klose, R.: Matlab implementation of the finite element method in elasticity. Computing **69**, 239–263 (2002)
2. Arnold, D., Awanou, G., Qiu, W.: Mixed finite elements for elasticity on quadrilateral meshes. Adv. Comput. Math. **41**, 553–572 (2015)
3. Arnold, D., Boffi, D., Falk, R.: Approximation by quadrilateral finite elements. Math. Comput. **71**, 909–922 (2002)
4. Brenner, S., Sung, L.-Y.: Linear finite element methods for planar linear elasticity. Math. Comput. **59**, 321–338 (1992)
5. Brenner, S.C., Scott, L.R.: The Mathematical Theory of Finite Element Methods. Texts in Applied Mathematics, vol. 15, Third edn. Springer, New York (2008)
6. Brezzi, F., Fortin, M.: Mixed and Hybrid Finite Element Methods. Springer, Berlin (1991)

7. Carstensen, C., Schedensack, M.: Medius analysis and comparison results for first-order finite element methods in linear elasticity. IMA J. Numer. Anal. **35**, 1591–1621 (2015)
8. Hu, J., Man, H., Wang, J., Zhang, S.: The simplest nonconforming mixed finite element method for linear elasticity in the symmetric formulation on n-rectangular grids. Comput. Math. Appl. **71**, 1317–1336 (2016)
9. Kozlov, V.A., Maz'ya, V.G., Rossmann, J.: Spectral Problems Associated with Corner Singularities of Solutions to Elliptic Equations. Mathematical Surveys and Monographs, vol. 85. American Mathematical Society, Providence (2001)
10. Lamichhane, B.P.: A mixed finite element method for nearly incompressible elasticity and Stokes equations using primal and dual meshes with quadrilateral and hexahedral grids. J. Comput. Appl. Math. **260**, 356–363 (2014)
11. Lamichhane, B.P., Stephan, E.P.: A symmetric mixed finite element method for nearly incompressible elasticity based on biorthogonal systems. Numer. Methods PDEs **28**, 1336–1353 (2012)
12. Lawrence Livermore National Laboratory. VisIt User's Manual, 1.5 edition (2005)
13. Li, H., Nistor, V.: LNG FEM: graded meshes on domains of polygonal structures. Contemp. Math. **586**, 239–246 (2013)
14. Liu, J., Cali, R.: A note on the approximation properties of the locally divergence-free finite elements. Int. J. Numer. Anal. Model. **5**, 693–703 (2008)
15. Liu, J., Tavener, S., Wang, Z.: The lowest order weak Galerkin finite element methods for the Darcy equation on quadrilateral and hybrid meshes. J. Comput. Phys. **359**, 312–330 (2018)
16. Mao, S., Chen, S.: A quadrilateral nonconforming finite element for linear elasticity problem. Adv. Comput. Math. **28**, 81–100 (2008)
17. Mijuca, D.: On hexahedral finite element hc8/27 in elasticity. Comput. Mech. **33**, 466–480 (2004)
18. Wang, C., Wang, J., Wang, R., Zhang, R.: A locking-free weak Galerkin finite element method for elasticity problems in the primal formulation. J. Comput. Appl. Math. **307**, 346–366 (2016)
19. Wang, J., Ye, X.: A weak Galerkin finite element method for second order elliptic problems. J. Comput. Appl. Math. **241**, 103–115 (2013)
20. Wheeler, M., Xue, G., Yotov, I.: A multipoint flux mixed finite element method on distorted quadrilaterals and hexahedra. Numer. Math. **121**, 165–204 (2012)
21. Yi, S.-Y.: Nonconforming mixed finite element methods for linear elasticity using rectangular elements in two and three dimensions. Calcolo **42**, 115–133 (2005)
22. Yi, S.-Y.: A new nonconforming mixed finite element method for linear elasticity. Math. Models Methods Appl. Sci. **16**, 979–999 (2006)
23. Zhang, S.: On the nested refinement of quadrilateral and hexahedral finite elements and the affine approximation. Numer. Math. **98**, 559–579 (2004)
24. Zhang, Z.: Analysis of some quadrilateral nonconforming elements for incompressible elasticity. SIAM J. Numer. Anal. **34**, 640–663 (1997)

Affiliations

Graham Harper[1] · Jiangguo Liu[1] · Simon Tavener[1] · Bin Zheng[2]

Graham Harper
harper@math.colostate.edu

Simon Tavener
tavener@math.colostate.edu

Bin Zheng
binzhengmath@gmail.com

[1] Department of Mathematics, Colorado State University, Fort Collins, CO 80523-1874, USA

[2] Beijing Institute for Scientific and Engineering Computing, Beijing 100124, China